



New Facies Model and Carbon Isotope Stratigraphy for an Ediacaran Carbonate Platform From South America (Tamengo Formation—Corumbá Group, SW Brazil)

Maria E. A. F. Ramos¹, Martino Giorgioni^{1*}, Detlef H. G. Walde¹, Dermeval A. do Carmo¹, Gabriella Fazio¹, Lucieth C. Vieira¹, Matheus Denezine¹, Roberto V. Santos¹, Rodrigo R. Adórno^{1,2} and Lucas Lage Guida¹

OPEN ACCESS

Edited by:

Michael Andrew Clare,
University of Southampton,
United Kingdom

Reviewed by:

Sabatino Ciarcia,
University of Sannio, Italy
Luca Basilone,
University of São Paulo, Brazil
Aram Bayet-Goll,
Institute for Advanced Studies in Basic
Sciences (IASBS), Iran

*Correspondence:

Martino Giorgioni
gmartino@unb.br

Specialty section:

This article was submitted to
Sedimentology, Stratigraphy and
Diagenesis,
a section of the journal
Frontiers in Earth Science

Received: 28 July 2021

Accepted: 17 May 2022

Published: 27 June 2022

Citation:

Ramos MEAF, Giorgioni M, Walde DHG, do Carmo DA, Fazio G, Vieira LC, Denezine M, V. Santos R, R. Adórno R and Lage Guida L (2022) New Facies Model and Carbon Isotope Stratigraphy for an Ediacaran Carbonate Platform From South America (Tamengo Formation—Corumbá Group, SW Brazil). *Front. Earth Sci.* 10:749066. doi: 10.3389/feart.2022.749066

¹Geosciences Institute, University of Brasília, Brasília, Brazil, ²Center for Technological Development-CEDES, Geological Survey of Brazil, Brasília, Brazil

The Ediacaran is a period characterized by the diversification of early animals and extensive neritic carbonate deposits. These deposits are still not well understood in terms of facies and carbon isotope composition ($\delta^{13}\text{C}$). In this study we focus on the Tamengo Formation, in southwestern Brazil, which constitutes one of the most continuous and well-preserved sedimentary record of the late Ediacaran in South America. We present new detailed lithofacies and stable isotopes data from two representative sections (Corcal and Laginha) and revise the paleoenvironmental and stratigraphic interpretation of the Tamengo Formation. The Corcal section consists of neritic deposits including shallow-water limestone beds, alternated with shale and subordinate marl beds. These facies yield specimens of the Ediacaran fossils *Cloudina lucianoi* and *Corumbella weneri*. On the other hand, the Laginha section shows more heterogeneous facies, such as impure carbonates, breccias, marls, and subordinate mudstone beds, as well as no evidence of *Corumbella weneri*. The stable carbon isotope record is also different between the two sections, despite belonging to the same unit. The Corcal section displays higher and more homogeneous $\delta^{13}\text{C}$ values, consistent with those of Ediacaran successions worldwide. The Laginha section, instead, displays more variable $\delta^{13}\text{C}$ values, which suggest the influence of local and post depositional processes. The difference between the two sections was attributed to the different distance from the shore. We propose that the difference is due to topographic variations of the continental platform, which, at the Laginha site, was steeper and controlled by extensional faults. Therefore, the Corcal section is a better reference for the Tamengo Formation, whereas the Laginha is more particular and influenced by local factors. Besides, the lithofacies associations of the Tamengo Formation are like those of the Doushantuo and Dengying formations, in South China, with no significant biogenic carbonate buildups, and different from those of other important Ediacaran units, such as the Nama Group in Namibia and the Buah Formation in Oman. Our work highlights the complexity and heterogeneity of Ediacaran carbonate

platforms and of their carbon isotopic composition. In addition, we characterize the Corcal section as a possible reference for the Ediacaran in South America.

Keywords: neoproterozoic, C and O isotopes, Paraguay Belt, Corcal, Laginha, carbonate ramp

1 INTRODUCTION

The Neoproterozoic geological record discloses a period of remarkable tectonic, climatic, and evolutionary changes on Earth. The paleogeographic modifications, related to Rodinia fragmentation followed by Gondwana assembly, are accompanied by glaciations and extensive volcanism, as well as major oceanic and climatic perturbations (e.g., Hoffman et al., 1998; Fike et al., 2006; Och and Shields-Zhou, 2012; Li et al., 2013; Gernon et al., 2016; Thallner et al., 2021). Furthermore, the fossil record reveals a noteworthy radiation of metazoans during the Ediacaran Period (e.g., Knoll and Carroll, 1999; Penny et al., 2014; Xiao et al., 2016; Kaufman, 2018; Gan et al., 2021).

The Ediacaran in general is characterized by climate warming and sea level rise following the major glaciations of the Cryogenian (e.g., Jiang et al., 2003a; Canfield et al., 2007; Kennedy et al., 2008; Le Heron and Craig, 2012; Lenton et al., 2014; Hohl et al., 2015; Wei et al., 2019). These conditions prompted the growing of carbonate platforms onto the inundated continental margins, as well as major perturbations in the carbon and sulfur cycles (e.g., Gorjan et al., 2000; Hurtgen et al., 2005; Elie et al., 2007; Halverson and Hurtgen., 2007; Ries et al., 2009; Johnston et al., 2012; Loyd et al., 2012; Crockford et al., 2016; Delpomdor et al., 2016; Tostevin et al., 2017; Zhang et al., 2018; Laakso et al., 2020; Yu et al., 2020). Therefore, Ediacaran carbonate sediments provide key information about the environmental and climatic conditions of this period, due to their high potential of preservation (e.g., Grotzinger and James, 2000). However, sedimentological studies on Ediacaran carbonates are challenging since they display several features with no analogues in the present-day, or even in the entire Phanerozoic (e.g., Grotzinger and Knoll, 1995; Chen et al., 2019; Hu et al., 2020; Riding and Virgone, 2020). This is true especially for the isotopic composition of carbon ($\delta^{13}\text{C}$), which yields values extremely anomalous, both positively and negatively (e.g., Kaufman and Knoll, 1995; Halverson et al., 2010; Grotzinger et al., 2011; Cui et al., 2018).

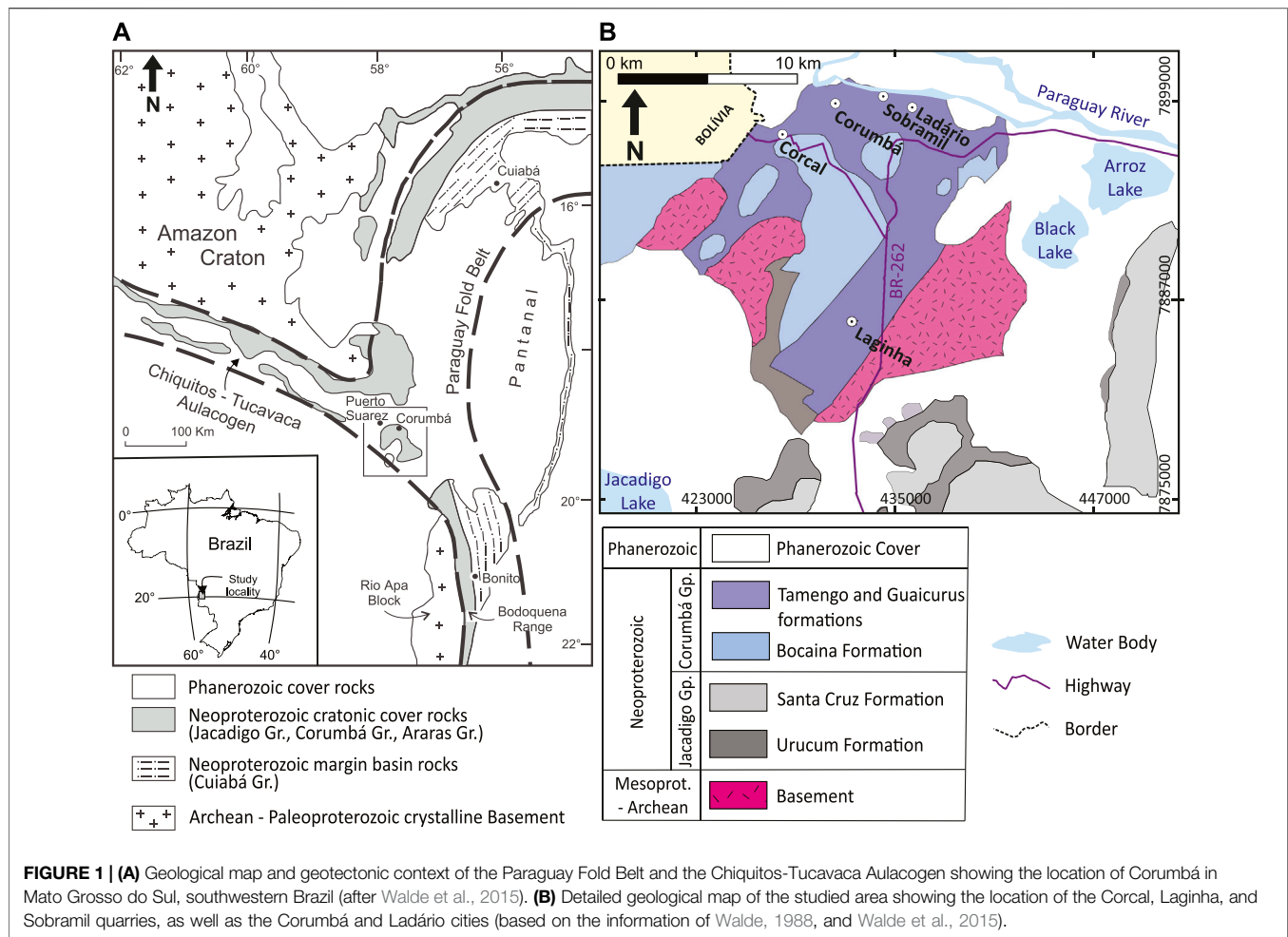
The origin of the Ediacaran $\delta^{13}\text{C}$ anomalies is still controversial, as they cannot be completely explained neither by primary nor by post depositional processes with the current state of knowledge. Indeed, there is evidence supporting either of the two possibilities (e.g., Fike et al., 2006; Bristow and Kennedy, 2008; Derry, 2010; Frimmel, 2010; Grotzinger et al., 2011; Shields et al., 2019; Husson et al., 2020; Xiao et al., 2020; Cui et al., 2021). This constitutes a major problem, as Ediacaran stratigraphic calibration is based mainly on carbon isotope chemostratigraphy (e.g., Narbonne et al., 2012; Xiao et al., 2016). Therefore, more detailed studies on Ediacaran carbonates are necessary to unravel the enigmatic origin of their carbon isotopic composition, as well as the

paleoenvironmental conditions in which the rise of the early animals on Earth occurred.

In Brazil, the most important Ediacaran geological record is the Tamengo Formation, of the Corumbá Group (Boggiani et al., 2010; Walde et al., 2015; Amorim et al., 2020). The importance of this unit comes mainly from the occurrence of upper Ediacaran guide fossils, such as *Cloudina luciano* and *Corumbella werneri* (e.g., Hahn et al., 1982; Adórno et al., 2017). However, this unit still lacks a detailed characterization of its depositional system, when compared with the main references for the Ediacaran period. Therefore, our main hypothesis is to test the potential of the Tamengo Fm. as a representative Ediacaran archive. In this work, we present new detailed stratigraphic sections and facies analyses of the Tamengo Formation, which provide an enhanced characterization of this Ediacaran carbonate paleoenvironment. The results reveal a heterogeneous ramp, deposited onto an irregular topography, in some parts influenced by extensional tectonics. In addition, we present new carbon and oxygen isotopes data that contribute to the validation of the Tamengo Formation's $\delta^{13}\text{C}$ curve as a possible chemostratigraphic reference for the Ediacaran in South America.

2 GEOLOGICAL SETTING AND LITHOSTRATIGRAPHY

The carbonate and associated siliciclastic sedimentary rocks of the Tamengo Formation (Corumbá Group) are exposed near the city of Corumbá, Mato Grosso do Sul, in western Brazil, close to the Bolivian border. These units are part of the succession of the southern portion of the Paraguay Belt, a thrust-and-fold belt generated during the Pan-African-Brasiliano orogenic cycle (de Alvarenga and Trompette, 1992; Boggiani et al., 1993; Trompette et al., 1998; Boggiani and Alvarenga 2004; Campanha et al., 2011; Meira, 2011). The Paraguay Belt extends for about 1,000 km with an approximate N-S orientation and is surrounded by the Amazon Craton to the North, the Pantanal Basin to the East, the Rio Apa Block to the South, and the Tucavaca-Chiquitos Aulacogen to the West. Jones (1985) and Walde (1988) consider that the Corumbá region sits on a tectonic triple junction, where the southern and northern branches of the Paraguay Belt intersect with the Tucavaca-Chiquitos Aulacogen (**Figure 1**). These basins formed after extensional tectonics related to the breakup of the Rodinia supercontinent, between 650 and 540 Ma (Babinski et al., 2013). This led to the evolution of a rift system, which formed the southern Paraguay Basin, filled with the sediments of the Jacadigo and Corumbá Groups of Neoproterozoic age (Trompette et al., 1998; De Alvarenga et al., 2009; **Figures 1, 2**). In the Early Paleozoic, the tectonic regime inverted, and these sequences were affected by the Brasiliano Orogeny, with ductile to brittle

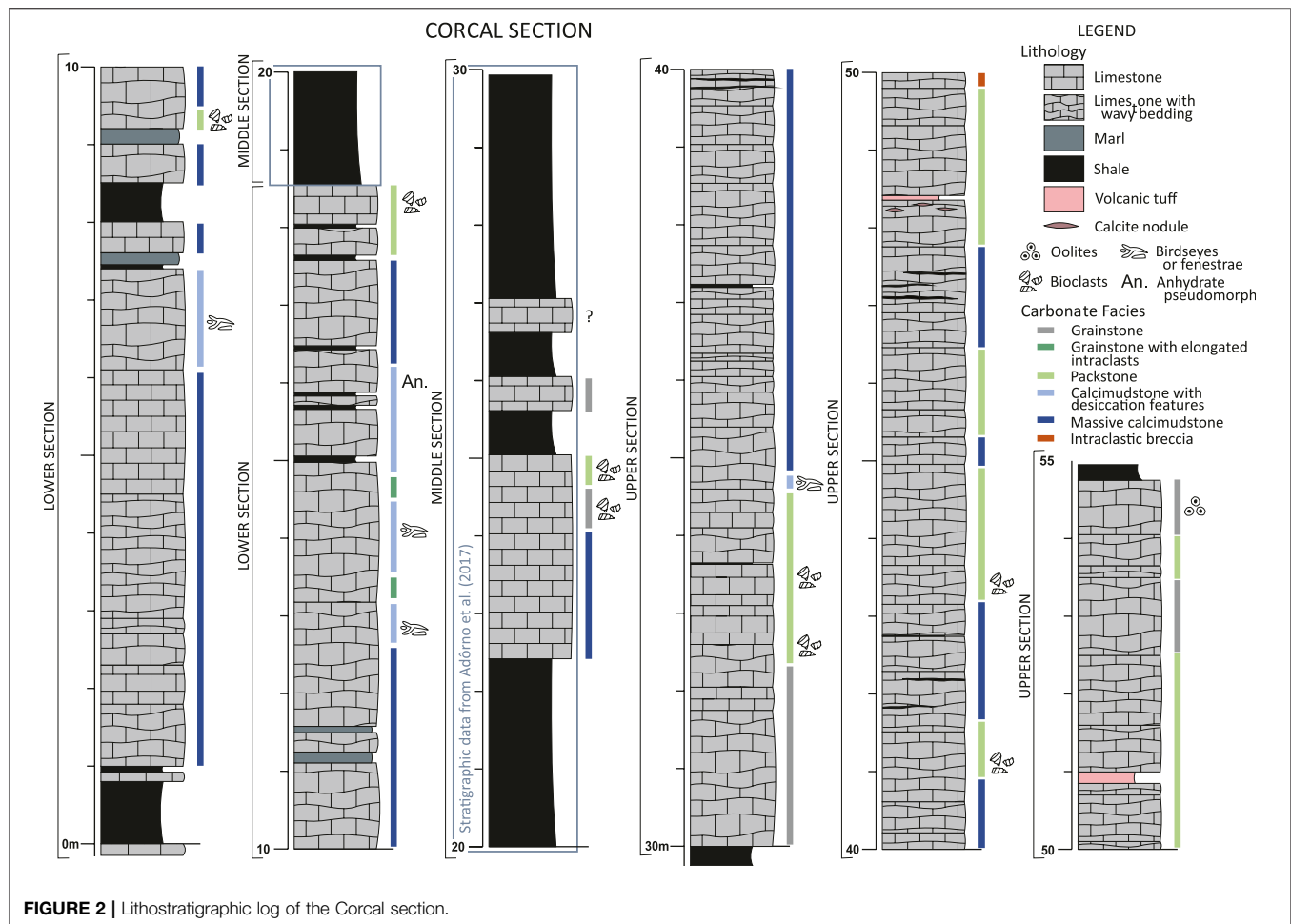


deformation and low-grade metamorphism, in greenschist facies (Trompette et al., 1998; D'el-Rey Silva et al., 2016).

The Jacadigo Group comprises diamictites, arkosic sandstones, and volcanic rocks of the Urucum Formation, at the base, followed by hematite-jaspilites with manganese rich horizons and dropstones of the Santa Cruz Formation, with minimum depositional age of 587 ± 7 Ma ($^{40}\text{Ar}/^{39}\text{Ar}$ in cryptomelane; Piacentini et al., 2013). The Corumbá Group includes carbonate and siliciclastic facies arranged in five units (Almeida, 1964; Almeida, 1965; Almeida, 1984; Boggiani, 1998; **Figure 1**). The Cadiueus and Cerradinho Formations form the lower part and consist of conglomerates, arkoses, siltstones, and occasionally limestones. These units of the lower Corumbá Group do not outcrop in the region of Corumbá. The overlying Bocaina Formation consists of stromatolitic dolostones and subordinate phosphorite levels, occurring with a wider spatial extent. These units are interpreted as a transgressive sequence, beginning with alluvial fan deposits (Cadiueus and Cerradinho Formations) followed by a vast tidal (Bocaina Fm.) flat with high evaporation rates (Boggiani, 1998; Oliveira, 2010; Fontanela, 2012; Sial et al., 2016). The upper part of the Corumbá Group is represented by the Tamengo and Guaicurus Formations. The former includes basal breccias and sandstones, followed by sets of dark fossil-rich limestones, alternated with marls and shales (e.g.,

Ramos et al., 2019). Dolostones and phosphorites occur locally. The paleontological content of the Tamengo Formation includes skeletal macrofossils, especially *C. luciano* (Beurlen and Sommer, 1957) an index species for the late Ediacaran (e.g., Grant, 1990; Adórno et al., 2017), and *C. werneri* (Hahn et al., 1982). Recently, a rich assemblage of ichnofossils, vendotaenids, and organic-walled microfossils was also described (e.g., Adórno, 2019). These fossil assemblages have drawn most part of the attention in the studies on the Tamengo Formation (Fairchild, 1978; Walde et al., 1982; Zaine and Fairchild, 1985; Zaine, 1991; Hidalgo, 2002; Gaucher et al., 2003; Kerber et al., 2013; Tobias, 2014; Walde et al., 2015; Adórno et al., 2017; Becker-Kerber et al., 2017; Parry et al., 2017; Walde et al., 2019; Diniz et al., 2021). *C. luciano* is usually found in limestones, whereas *C. werneri* occurs in shales (Adórno et al., 2017; Oliveira et al., 2019; Adórno, 2019; Amorim et al., 2020).

Boggiani (1998) suggests that the Tamengo Formation formed above the Bocaina Formation during a transgression, establishing a slope-break ramp system marked by reworking of the shallower sediment. On the other hand, Oliveira et al. (2019) and Amorim et al. (2020) propose a shallower setting, with oolitic bars and storm-derived deposits. The overlying Guaicurus Formation consists of laminated siltstones, which mark the end of carbonate deposition, related to climatic or tectonic changes. This unit was probably



deposited in a deeper environment, below the storm wave base (Boggiani, 1998; Gaucher et al., 2003; Oliveira, 2010). The boundary between the Tamengo and Guaicurus formations is still controversial, as it probably contains a hiatus and then the transition to the Cambrian (Adórno et al., 2019a; Fazio et al., 2019).

Concerning the age of the Corumbá Group, U-Pb dating of zircons from volcanic ash by Parry et al. (2017) provide ages of 555.18 ± 0.7 Ma for the top of the Bocaina Formation and $\sim 542.37 \pm 0.7$ Ma for the top of the Tamengo Formation. These ages agree with the 543 ± 3 Ma provided before by Babinski et al. (2008). Furthermore, the presence of the index-fossils *C. luciano* and *Cloudina carinata* in the Tamengo Formation supports an upper Ediacaran age (Adórno et al., 2017; Adórno et al., 2019b).

3 METHODOLOGY

3.1 Fieldwork and Lithostratigraphy

The studied outcrops are in two limestone quarries near the city of Corumbá, in western Brazil. The Corcal and Laginha sections were selected for their vertical continuity, fresh rock exposures, accessibility, and availability of previous studies.

These sites were visited in June 2018 and detailed lithostratigraphic logs were measured and described with a cm to dm resolution (Figures 2, 3). A total of 225 samples were collected for petrographic characterization and geochemical analyses. Outcrops conditions allowed for collecting samples bed by bed. In case of lenticular or amalgamated beds, the samples were collected considering a thicker interval, in order not to confuse the stratigraphic relationships. The average sample spacing resulted of ~ 20 cm. Some intervals were completed using the lithostratigraphic logs of Adórno et al. (2017) and Fazio et al. (2019), as highlighted in Figures 2, 3. This choice was taken for intervals that were already sufficiently detailed in these previous studies, or that were not possible to access.

3.2 Petrography

Petrographic characterization was performed using a ZEISS petrographic microscope at the University of Brasília (UnB). Seventy-nine thin sections were studied, being 40 from the Corcal and 36 from the Laginha section (Supplementary Material). A plain white paper was placed underneath the thin section and used as a light diffuser to clarify textural features under the microscope (Delgado, 1977).

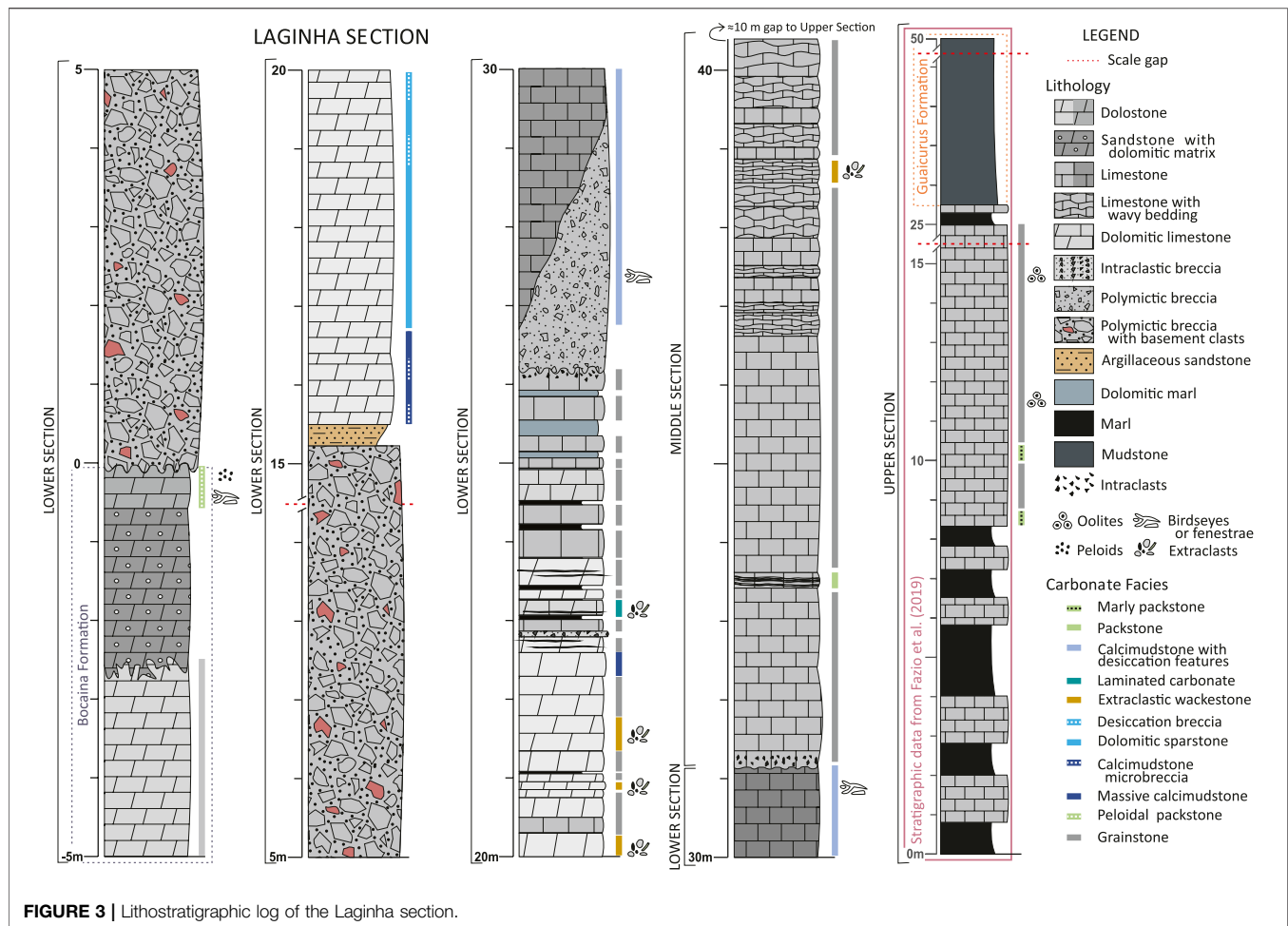


FIGURE 3 | Lithostratigraphic log of the Lágina section.

The classification of the carbonate lithofacies was done according to Wright (1992) and Flügel (2004) on the base of: 1) texture, considering the amount of matrix respect to other constituents; 2) composition, based on the mineralogy and the type of grains; 3) sedimentary structures. Therefore, the name represents the main textural features, and the adjectives refer to composition and structures (i.e., “massive calcimudstone”, “dolomitic sparstone”, “intraclastic breccia”).

The Wentworth (1922) grain size classification was used for the siliciclastic facies. Besides, “shale” and “mudstone” were differentiated, as the former displayed fissile or foliated structure and calcite filled veins, which were absent in the latter. Facies associations were defined according to the carbonate ramp model of Burchette and Wright (1992).

3.3 Scanning Electron Microscopy

After the analysis at the optical petrographic microscope, which allowed for identifying constituents that needed a more detailed characterization, nine thin sections were selected among the representative lithofacies for SEM analyses. Prior to the analysis the sections were coated with carbon, and then analyzed at the University of Brasília (UnB) using a FEI QUANTA 450 scanning electron microscope with

a BSE detector, 20 kV accelerating voltage, working distance of 10–12 mm, and in high-vacuum mode.

3.4 Carbon and Oxygen Isotopes Geochemistry

For carbon and oxygen isotopes analysis in carbonate ($\delta^{13}\text{C}$ and $\delta^{18}\text{O}$), 116 samples from Corcal and 54 from Lágina were collected with 20–40 cm spacing. The respective lithofacies was always annotated alongside each sample, to constrain the interpretation of the results. Additionally, areas containing veins, fractures, and other post-depositional features, likely to interfere with the primary isotopic signal, were avoided. Fresh rock samples were powdered using a drill with a 3 mm-diameter bit. Prior to the analysis about 300 μg of material were put in glass vials, acclimatized at 72°C, and flushed with He to eliminate atmospheric gases. Afterwards, carbonate samples were reacted with concentrated phosphoric acid during 1 h, and the released CO_2 was analyzed with a Thermo® Gasbench II connected to a Thermo® Delta V^{Plus} mass spectrometer at the University of Brasília (UnB). The isotopic ratios are reported in per mil (‰), using the conventional δ notation, relative to the Vienna Pee Dee Belemnite (VPDB) standard. The analytical precision is $\pm 0.1\%$ for both $\delta^{13}\text{C}$ and $\delta^{18}\text{O}$.

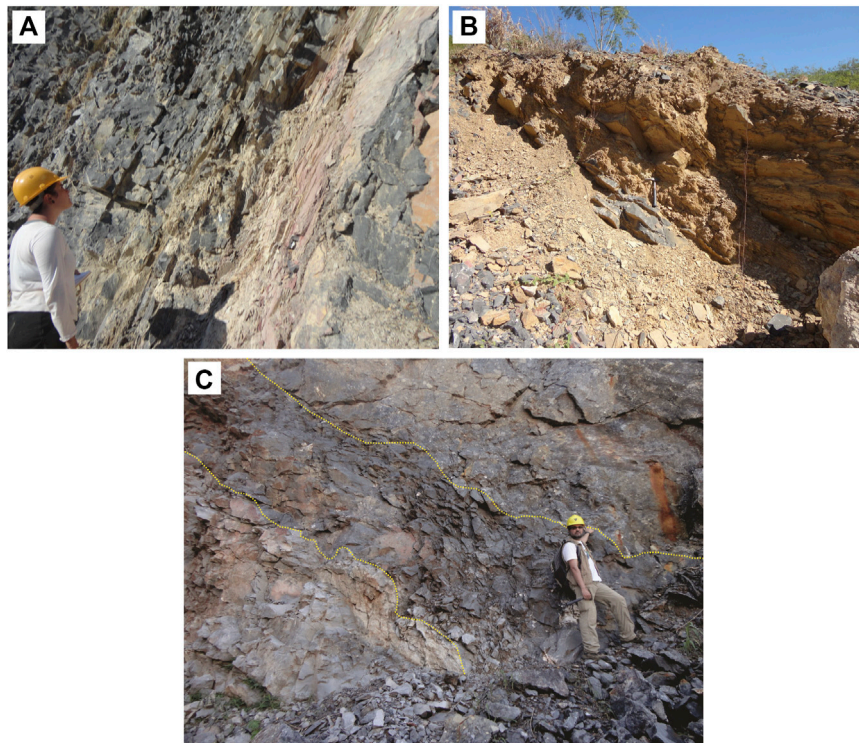


FIGURE 4 | (A) Limestones and marls in the lower part of the Corcal section. **(B)** Shale layer in the middle part of the Corcal section. **(C)** Basal part of Laginha section displaying the contact between the Bocaina and Tamengo formations. From bottom to top: light gray dolomitic grainstone, first erosional contact, dark gray sandstone with dolomitic matrix grading upward into dark gray peloidal packstone, second erosional contact, homogeneous polymictic breccia with basement clasts. Erosional contacts are highlighted by yellow dotted lines.

4 RESULTS

4.1 Corcal Section

The Corcal section is 55 m thick and consists of m-thick bundles of shallow-water limestone with tabular to wavy amalgamated beds and cm-thick beds of mudstone and marl, alternating with m-thick intervals of shales (Figures 2, 4). Neither the base nor the top of the Tamengo Formation is exposed at this site. The lower and upper parts of the section were logged in the northern and southern side of the quarry, respectively. On the other hand, the middle part was completed using the log by Adórno et al. (2017), as it was considered sufficiently detailed after verification in the field. The split of the profile in these three sub-sections was done to avoid parts that occurred tectonically disturbed by faults and folds, which deformed especially the most ductile shale beds. However, the stratigraphy was adequately exposed for allowing the recognition of the entire succession in continuity.

The lower part of the section (from 0 to 18.60 m) consists of shallow-water limestones organized in 1–2 m thick bundles of wavy and amalgamated beds alternated with bundles of cm- to dm-thick tabular beds (Figures 2, 4). At the microscopic scale, the limestones in this interval consist mainly of calcimudstones, often recrystallized, with some extraclasts of quartz and mica, bioclasts, and intraclasts (Figure 5). Generally, they display a

massive structure, but locally evidence of desiccation can be observed, such as birdseyes, anhydrate pseudomorphs, silicification, dolomitization, and micritization (Figures 5B,C,G). Alongside the calcimudstones, there are minor occurrences of packstones and grainstones formed by bioclasts, intraclasts, and siliclastic extraclasts (Figures 5D,H–J). Grain size is from sand to granule and the intergranular space is filled with micrite or calcite cement. Occasionally recrystallization or dolomitization is present. The structure is massive, with lenticular veins and calcite-filled fractures. In few cases the grainstones display angular and variously elongated intraclasts, sometimes with combining edge, and local ferruginous matrix, suggesting possible brecciation by desiccation. The limestone succession is interrupted by few centimeter to decimeter thick beds of shales and marls, formed by clay to silt-size detrital grains, especially quartz, with massive to finely laminated structures and variable carbonate, occurring as cement or microscopic nodules (Figure 5E). Fazio et al. (2019) noted also the presence of gypsum pseudomorphs.

The middle part of the section (from 18.60 to 29.90 m) consists mainly of massive shales, interrupted by a 2.25 m thick and two decimeter thick limestone beds. The shales are siliclastic mudstone, sometimes thinly laminated, with minor quartz grains and carbonate cement (Figure 4B). There are rare

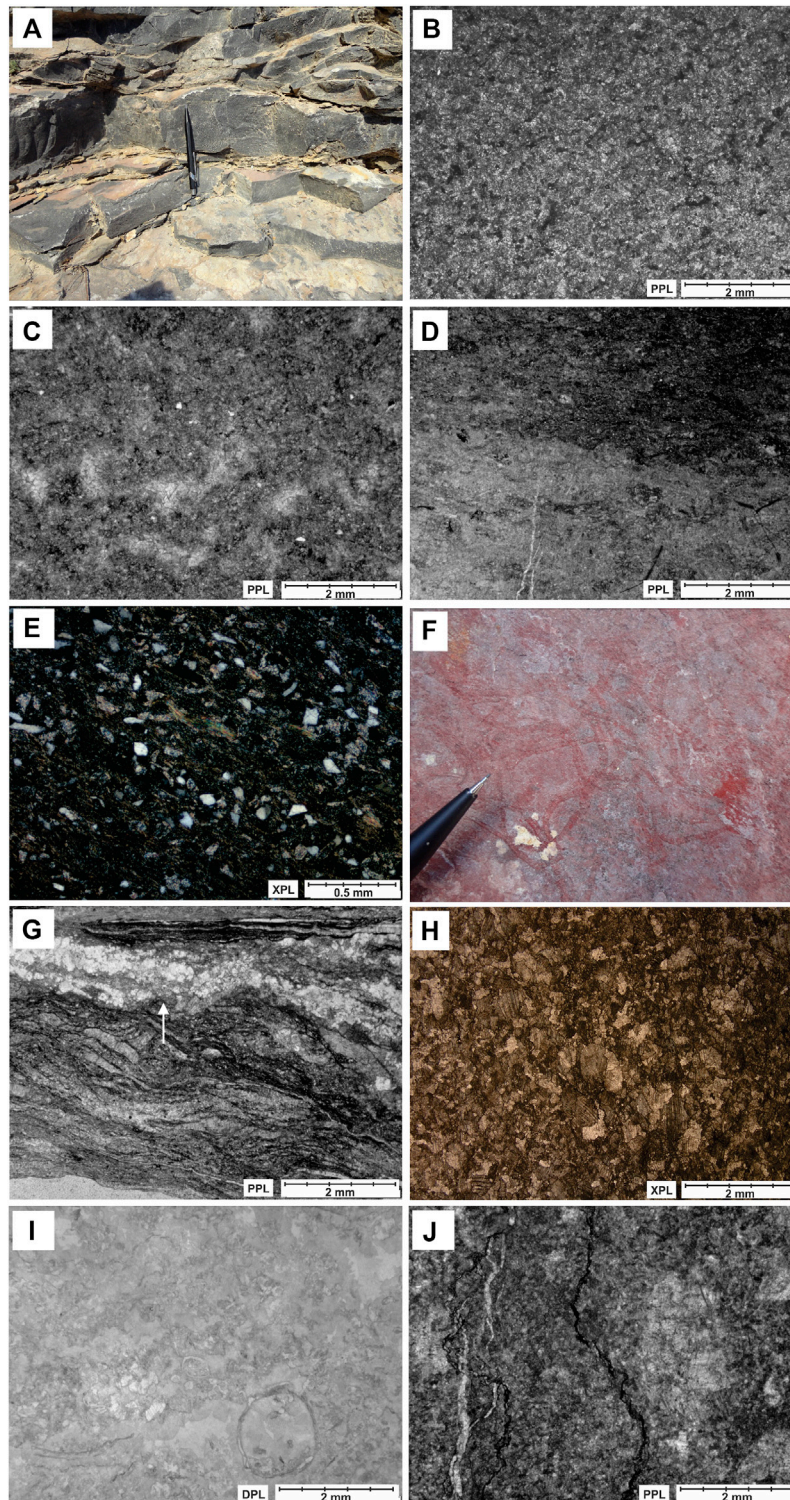


FIGURE 5 | Lithofacies of the Corcal section: **(A)** Limestone beds in the upper part of the section (scale object is 13 cm). **(B)** Thin section view of a massive calcimudstone (b/w; Sample C1 2,62). **(C)** Fenestral structures filled with calcite cement (b/w; Sample MP 2118). **(D)** Thin section view of an intraclastic grainstone with local ferruginous matrix (b/w; Sample MP 2119). **(E)** Thin section view of a marl (Sample MP 2115). **(F)** Specimens of *C. wernerii* preserved along a surface in a shale bed (scale object is 2 cm). **(G)** Calcimudstone with elongated intraclasts and silicified anhydrite pseudomorphs, indicated by arrow (b/w; Sample MP 2123). **(H)** Recrystallized grainstone (Sample C3 24,60). **(I)** Grainstone with bioclasts of *Cloudina* (b/w; Sample MP 2128). **(J)** Recrystallized packstone (b/w; Sample MP 2132).

opaque grains, compaction-related segregation structures, calcite and quartz-filled fractures, and silicified nodules. These are also the lithological intervals yielding the fossils of *C. wernerii*, indicating the upper Ediacaran age of the Tamengo Formation (Figure 5F; Adorno et al., 2017). The limestone beds consist of calcimudstones and grainstones, similar to those in the lower part of the section.

The upper part of the section (from 29.90 to 54.40 m) consists of limestone arranged in sets of centimeter to decimeter thick beds, varying from tabular to wavy, interchanged with rare millimeter to centimeter thick shale beds, and, occasionally centimeter thick mudstone lenses (Figure 5A). Amorim et al. (2020) also described hummocky cross stratification in correlative outcrops of this interval. As this kind of sedimentary structure is generally highlighted by weathering on the surface of the rock, it is not visible in the Corcal section because the surface of the outcrop is too fresh, being it in an active quarry. At microscopic scale the limestones consist of calcimudstone and grainstone with intraclasts and bioclasts of *Cloudina* type organisms, as suggested by the tubular shapes (Figures 5H,I). At 34.65 m birdseye porosity was noted, and at 48.00 and 50.50 m there are tabular centimeter thick beds of light, greenish to whitish, clayey sediment, different from the other mudstones, described as possible volcanic tuffs. In addition, at 48.13 m there are pinkish centimetric calcite nodules, and a layer of intraclastic breccia was observed at 49.66 m. The uppermost limestone bed is a massive oolitic grainstone and, above, starts a massive interval of shales with carbonate lenses, described in detail by Fazio et al. (2019). SEM analysis revealed also the presence of fluorapatite in 4 different levels of the Corcal section: 6.50, 10.40, 2.55, and 18.42 m.

4.2 Laginha Section

The Laginha section is about 100 m thick and displays both the lower and the upper boundaries of the Tamengo Formation. The succession yields a higher variety of lithofacies than the Corcal section (Figure 3).

The lower part of the section (from -5 to 30 m) starts with a dolomitic interval, formed by 2.50 m thick massive bed of light grey grainstone, followed by ~2.00 m of massive dark gray sandstone with dolomitic matrix mostly composed of very well-rounded quartz grains with approximately equal amounts of grains and matrix. Above, there is ~0.5 m thick peloidal packstone with fenestral pores, filled with spathic calcite. The contact between the latter two beds is very irregular, indicating an erosional and possibly karstified unconformity (Figure 4C). This interval represents the uppermost part of the Bocaina Formation (Boggiani, 1998). The Tamengo Formation starts with a ~15 m thick bed of massive polymictic breccia containing various types of intraclasts and extraclasts with composition of quartz, dolostone, limestone, chert, phosphorite, and granite type rocks. They are poorly sorted, with chaotic distribution and with a rounded to very angular shape. The matrix is dolomitic and dark gray, there are irregular voids filled with white spathic calcite (Figure 6A). The contact at the base is erosional. Above the thick polymictic

breccia there is a 25 cm thick friable yellowish-brown, massive argillaceous sandstone, with sand-size quartz grains and lithoclasts within an argillaceous matrix (Figures 6B, 7A, 8A,B).

Upwards occurs a mainly carbonate succession, starting with 4.5 m of massive dolostones with numerous randomly oriented fractures, with millimeters to centimeters size and filled with white sparry calcite (Figure 8C). Above, there are 2.80 m of sparstones, arranged in sets of centimeter to decimeter thick tabular beds, dolomitic to calcitic, massive to laminated, containing stylolites and calcite-filled veins, locally brecciated and associated with fluorite (Figures 6C,D, 7D). The succession continues with alternating dolostones and limestones, consisting of laminated facies, with alternating crystalline and sandy laminae, the formers are calcitic to dolomitic, with sparse extraclasts of quartz and mica; and the latter are grain-supported, with calcitic to dolomitic matrix and sand-size extraclasts varying in composition from quartz to k-feldspar (Figures 6E,F, 7B, 8D-G). Authigenic pyrite and phosphatized grains are present, and SEM-EDS analyses revealed traces of zircon and possible anatase. Late compaction structures, such as stylolites and calcite-filled veins, occur frequently. In addition, there are massive wackestones with micritic matrix and abundant extraclasts, especially quartz and muscovite, ranging from fine to coarse sand-size; and grainstones formed predominantly by concentric ooids, occurring as single or composite, often micritized or completely recrystallized, with rare aggregate grains and cemented by calcite. At 22.75 m there is a 7 cm thick bed of intraclastic breccia, grain-supported, with micritic matrix and angular intraclasts, ranging in size from fine sand to granule, with the larger grains of tabular shape, and with abundant fine quartz grains (Figure 7C).

At 26.40 m occurs an irregular massive polymictic breccia, with maximum thickness of 5 m and erosional contact at the base, which laterally meets a light gray limestone in angular unconformity (Figure 7E). It is grain-supported, with limestone intraclasts and grains varying from quartz to dolomite, phosphorite, mudstone, k-feldspar, and pyrite, with micritic matrix. It is worth noting the absence of coarse granitoid clasts from the basement, observed in the breccia at the base of this unit (Figure 6G).

The middle part of the section (from 30 to ~44 m) starts with 5.35 m of dark gray limestone, overlying the breccia with a very irregular, erosional, and perhaps karstified contact. This interval is massive, consisting of calcimudstones micritized to recrystallized, with fenestral pores and chert nodules; alternatively, they occur mottled, dolomitized, with quartz and opaque extraclasts, and calcite-filled fractures. Sometimes they are brecciated, with fractures and very angular intraclasts, with isopachous or dog tooth cement at the margins and syntaxial cement at the center (Figures 8H-L). The last 3.75 m thick interval of the middle section consists of dark gray limestones arranged in sets of centimeters to decimeters thick beds, varying from tabular to wavy. Microscopically they are oolitic grainstones, with local occurrences of micritic matrix and extraclasts (Figures 7F, 8M-O).

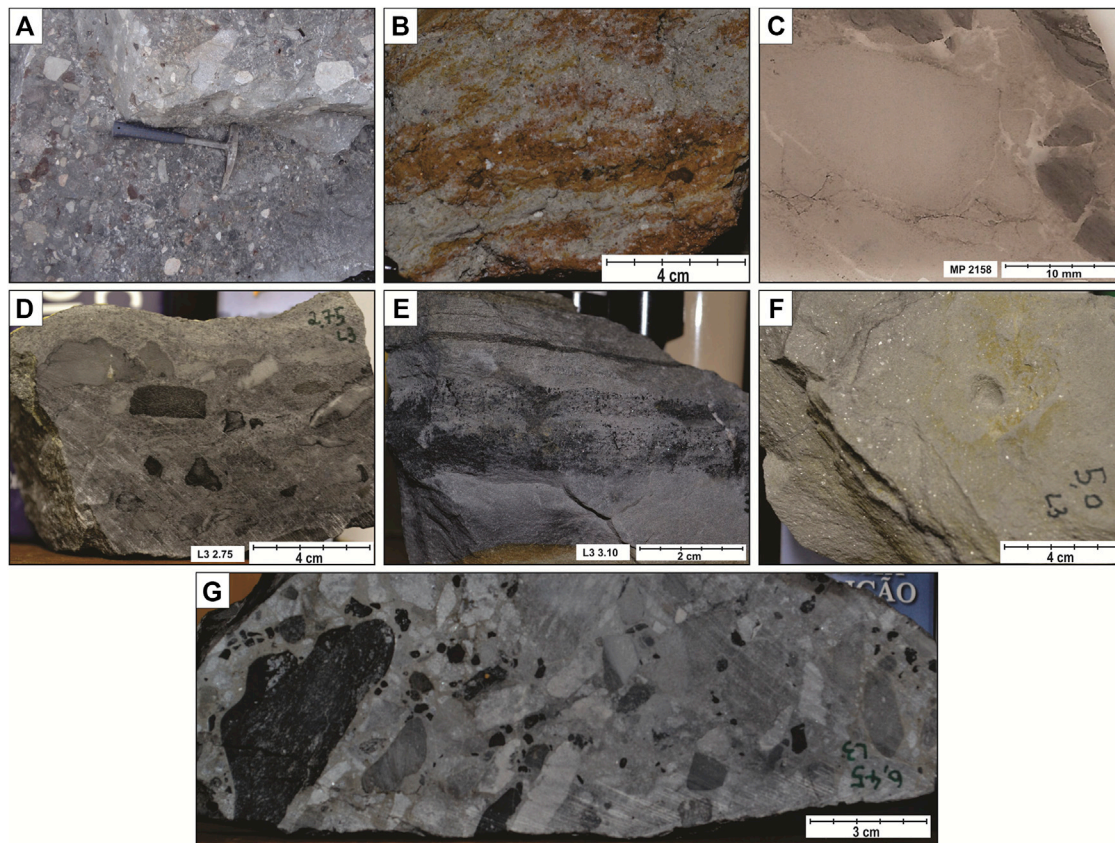


FIGURE 6 | Macroscopic view of sedimentary facies in the lower part of the Laginha section. Sample identification and scale at the right-hand bottom corner of each picture. **(A)** Basal polymictic breccia with basement clasts, poorly sorted and with micritic matrix. **(B)** Muddy sandstone with quartz grains and lithoclasts. **(C)** Thin section photograph of a dolomitized desiccation breccia. Note the broken dark grains still positioned next to each other counterparts. **(D)** Intraclastic breccia with square, angular clasts. **(E)** Laminated carbonate with alternated finer and coarser layers. **(F)** Dolomitic marl displaying mica extraclasts. **(G)** Polymictic intraclastic breccia with homogeneous structure.

During the fieldwork we could not access to the upper part of the section, and thus we completed the log with that of Fazio et al. (2019). However, with the stratigraphic information available it was not possible to precisely link the middle to the upper part of the section and a 10 m gap is estimated between the two. According to Fazio et al. (2019), the upper part of the section comprises 30 m, with the lower half consisting of alternating limestones and laminated mudrocks, with a composition ranging from carbonate to siliciclastic. Above this interval, in conformable or para conformable contact, there are ~24 m of pure siltstone, with millimeters to centimeters thick, plane parallel to wavy lamination, belonging to the Guaicurus Formation. The contact between the two formations in the Laginha section presents 1 m-thick non-cohesive yellowish beige siltstone with kaolinite and gypsum among its mineralogy (Fazio et al., 2019).

4.3 Carbon and Oxygen Stable Isotopes Geochemistry

The Corcal section displays little dispersed $\delta^{13}\text{C}$ values (Figure 9), ranging from 0.70‰ to 6.97‰. In the lower part

of the section, the values increase gradually from ~3.5‰ to ~5‰, and then persist through the middle and upper part. There are minor positive peaks of 5.33‰, 6.97‰, and 5.75‰ at 10, 12.95, and 15.95 m, respectively, and a negative peak of 4.16‰ at 32.85 m, as well as few outliers. $\delta^{18}\text{O}$ values range from -10.47‰ to -4.75‰. In the lower part of the section values are more dispersed but become steadier in the middle and upper part. The cross-plot between $\delta^{13}\text{C}$ and $\delta^{18}\text{O}$ shows no linear correlation or facies-related clustering (Figure 10).

The Laginha section yields $\delta^{13}\text{C}$ values from -3.11‰ to 4.92‰ (Figure 9). In the Bocaina Formation the values show a linear increase from 1.53‰ to 3.14‰. Above the polymictic breccia, which was not analyzed for stable isotopes, values start at 0.79‰ and decrease to -3.00‰ at 21 m, then increase again to 0.13‰ at 27.35 m and 1.92‰ at 30.75 m. In this last interval the values are scattered, showing no clear trend. The middle part of the section has values around -1.00‰, with a distinct negative peak of -2.14‰ at 34.8 m. The upper part of the section has a lower sampling resolution, however, a rough trend can be observed with values starting around 4‰, increasing to 4.80‰ at 12 m, and then decreasing to around 2‰ from 17 m to the top of the Tamengo

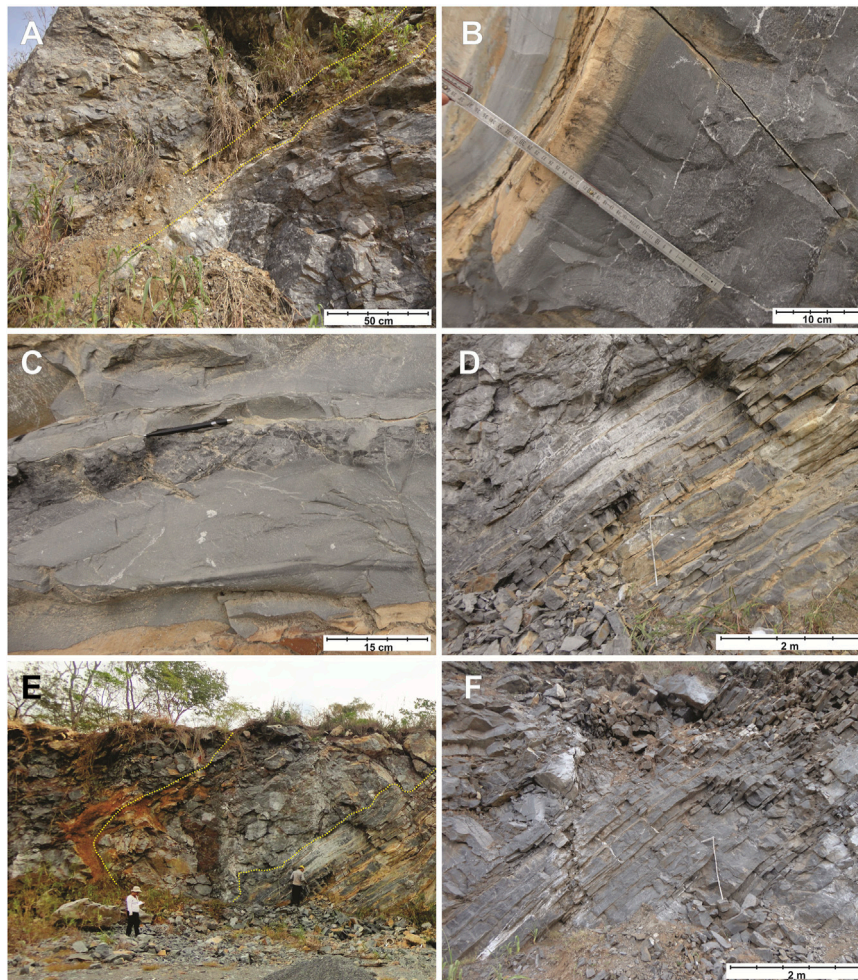


FIGURE 7 | Macroscopic lithofacies of the Laginha section. **(A)** Polymictic breccia overlaid by muddy sandstone and then carbonate beds. **(B)** Sequence of dark gray fine grainstone, dark gray coarse lithic sandstone with carbonate matrix, and light gray dolomitic wackestone. **(C)** Cm thick layer of intraclastic breccia in the lower section. **(D)** Limestones with dm thick tabular bedding in the lower section. **(E)** Homogeneous, polymictic intraclastic breccia within dark gray limestones. **(F)** Limestones with dm thick tabular bedding in the upper part of the lower section, with chaotic bedding towards the top.

Formation. The average is -1.01% in the lower and middle part of the section, and 3.29% in the upper part. $\delta^{18}\text{O}$ values range from -10.09% to -2.12% , with average of -6.84% . They are dispersed, showing no clear trend, within the lower and middle part of the section, and range between -8% and -6% in the upper part. The cross-plot between $\delta^{13}\text{C}$ and $\delta^{18}\text{O}$ shows no linear correlation or facies-related clustering (Figure 10).

5 DISCUSSION

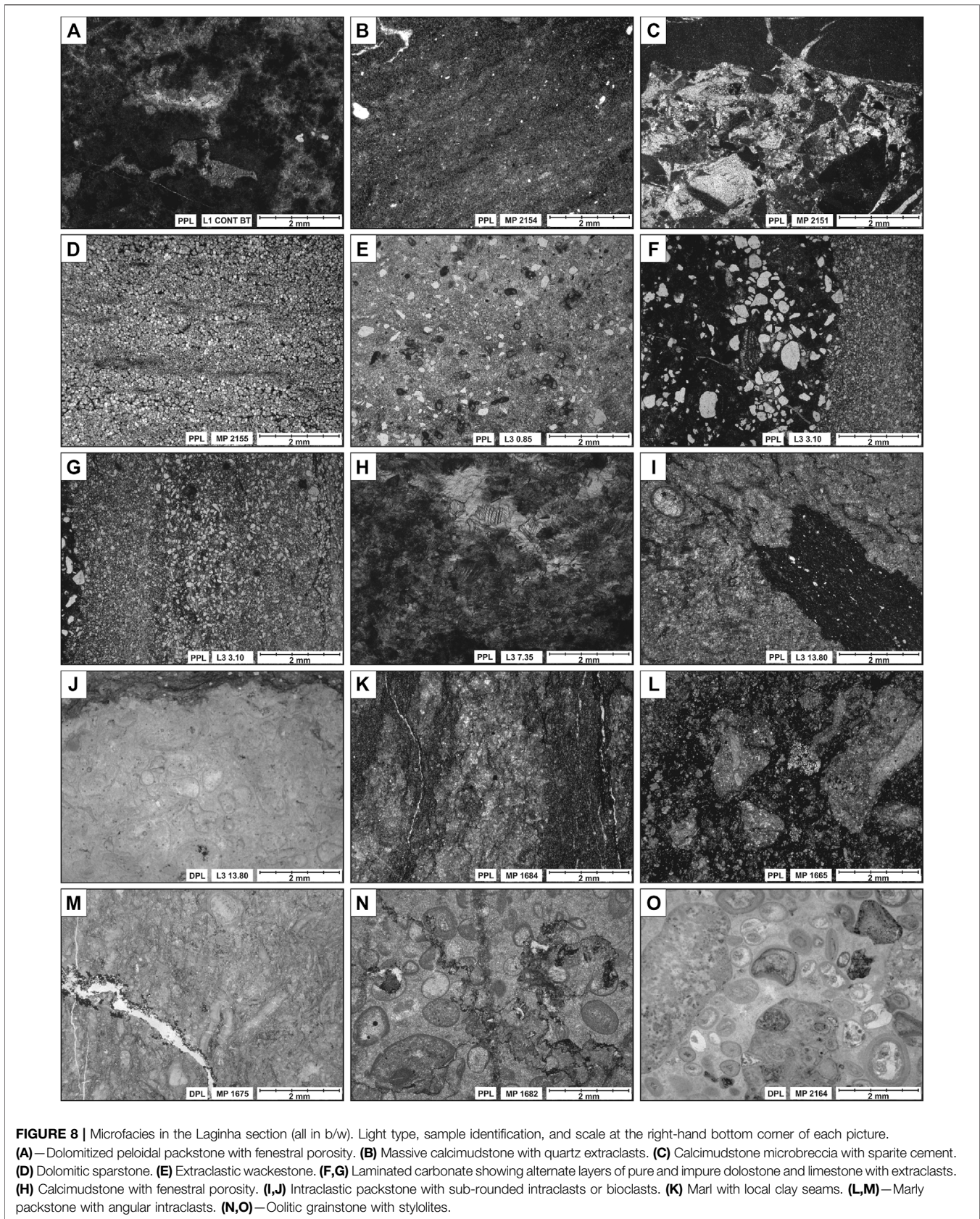
5.1 Facies Interpretation

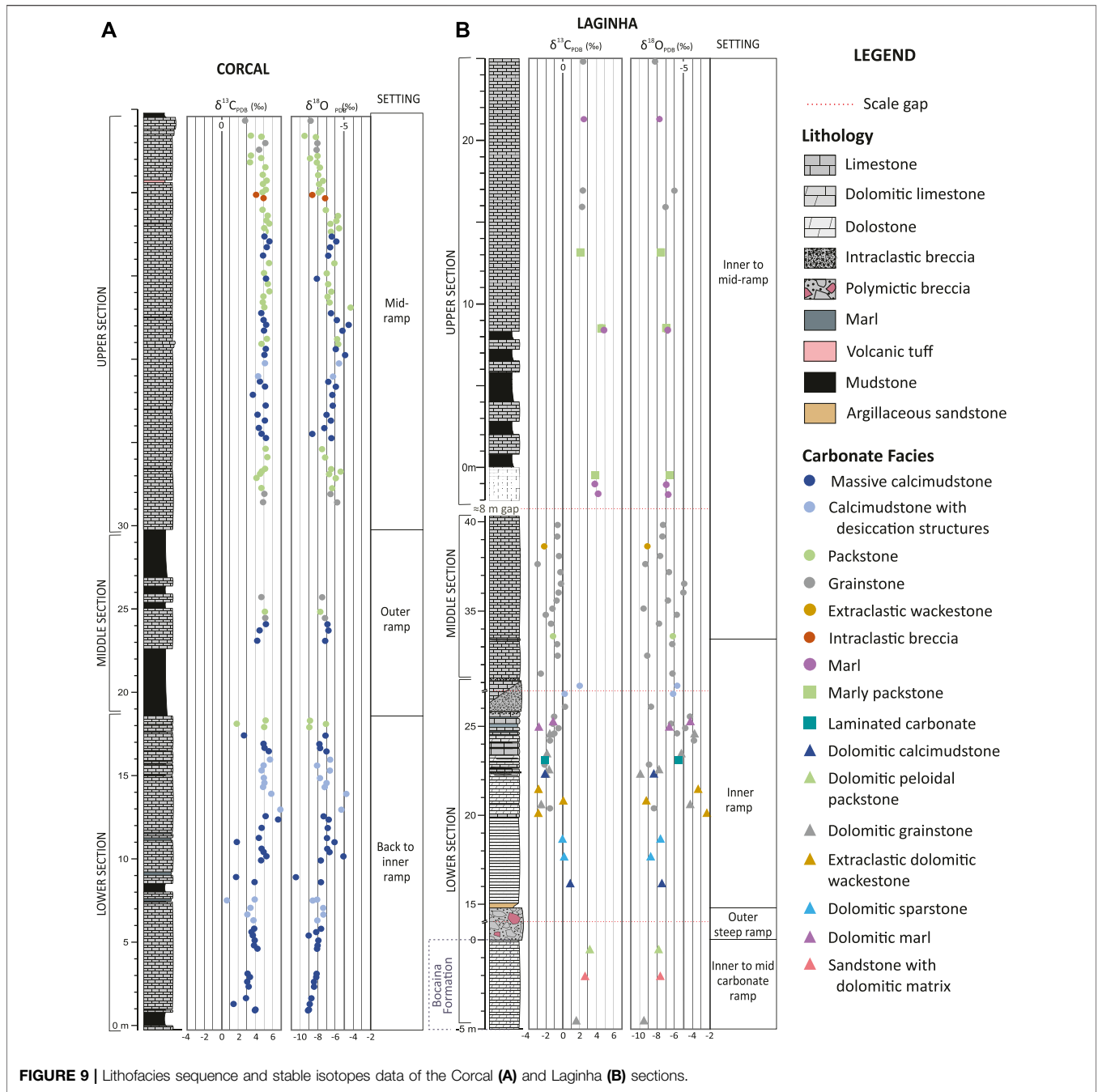
5.1.1 Corcal Section

In the Corcal section were recognized nine sedimentary facies, listed in Table 1. The lower part is dominated by the facies C1, alternated with C4, with the occurrence of C2 and C3. This facies association suggests a shallow low-energy environment, dominated by the settling of fine-grain sediments, with the

supply of coarser carbonate grains reworked by waves or currents. Episodic influx of siliciclastic material and of emersion and desiccation also occurred (Tucker and Wright, 1990; Schlager, 2005; Łabaj and Pratt, 2016). Silicification, observed in some levels, also supports this interpretation, as silica is supplied by continental runoff and then, during diagenesis, gets mobilized and fills the cracks opened by the desiccation (Laschet, 1984 in Flügel, 2004). This evidence suggests a back to inner ramp environment for the lower part of the Corcal section (Burchette and Wright, 1992).

The shales dominating the middle part of the Corcal, facies C8, represent a significant decreasing of the energy and of the carbonate input. They can be attributed to episodes of relative sea level rise, in which the flooded carbonate factory decreased its productivity, and the environment reached higher depths, below the storm wave base (Walker, 1984; Łabaj and Pratt, 2016; Oliveira et al., 2019; Amorim et al., 2020; Ding et al., 2021). The limestone intervals within the shales display facies C1, C5,



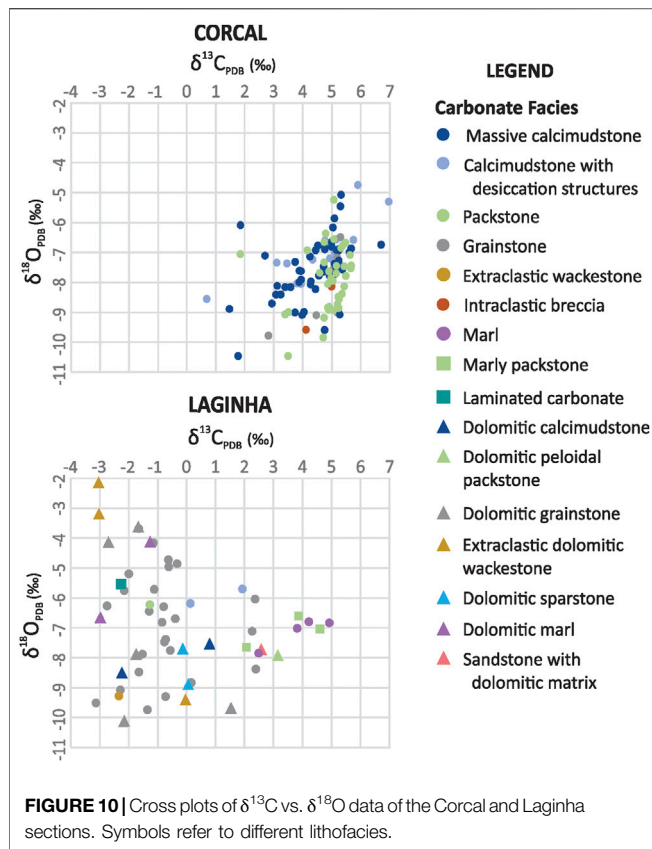


and C6, indicative of higher energy conditions that can be attributed to a mid-ramp setting (Burchette and Wright, 1992; Schlager, 2005). Therefore, they can represent higher frequency cycles of carbonate platform recovery and progradation during the transgressive phase.

The facies succession in the upper part of the Corcal section consists of facies C5, C6, C7, with local occurrence of C2 and C9. It indicates an active carbonate factory and higher energy conditions than the underlying sequence. It can be related to a mid-ramp carbonate platform environment, with depth mainly below and sometimes above the fair-weather wave base (Burchette and

Wright, 1992). This interval may represent the carbonate platform recovery and progradation during the sea level high stand, after the rise (Schlager, 2005; Łabaj and Pratt, 2016).

The volcanic tuff beds of facies C9 might be related to a nearby volcanic eruption. The ashes could have been transported by winds and currents and redeposited by settling or low-density gravity flows (Nichols, 2009). The volcanic activity could be related to the extensional tectonics occurring in the Corumbá region during the Ediacaran (Alvarenga et al., 2011; Warren et al., 2019). These, volcanic tuff beds were described in previous studies, such as Boggiani et al. (2010) and Amorim et al. (2020),



and dated by Babinski et al. (2008) and Parry et al. (2017) providing ages of 543 ± 3 Ma and 541.85 ± 0.75 Ma, respectively.

5.1.2 Laginha Section

The Laginha section displays a greater variety of lithofacies than the Corcal, as 18 were recognized and listed in **Table 2**. The karstified surface above the dolomitic grainstone (facies L1) in the upper Bocaina Formation can be evidence of emersion, and the very well rounded and sorted grains of the overlaying sandstone bed (facies L2) suggest long distance transport and possible reworking by beach waves (Tucker and Wright, 1990). Besides, peloids occurring in the overlaying facies L3 are typical of shallow, low energy restricted marine conditions (Tucker and Wright, 1990; Flügel, 2004). Hence, these units can represent a peritidal environment developed after a local regression, as suggested also by Boggiani (1998) and Oliveira (2010).

The thick polymictic breccia with basement clasts at the base of the Tamengo Formation constitutes the facies L4 (**Figure 3**). Breccia facies in carbonate platforms may be due to multiple factors. Storm episodes can produce breccias, however, in this case they are clast supported and occur in beds with maximum thickness of few meters and interbedded with fine offshore facies (e.g., Seguret et al., 2001; Wang et al., 2019). The breccia at the base of the Tamengo Formation is very poorly sorted, contains abundant matrix and basement clasts, indicating continental erosion occurring nearby the carbonate platform. Its thickness higher than 10 m and massive structure resemble the breccias

described in the Otavi Group in Namibia (Eyles and Januszczak, 2007). This is one of the most studied successions of the Neoproterozoic and the breccias are interpreted as related to extensional tectonic (Eyles and Januszczak, 2007). The same interpretation was given to similar breccia deposits of Cretaceous age in the Northern Calcareous Alps (Sanders and Höfling, 2000). Considering that the Corumbá Group is interpreted as part of a rift filling sequence, this polymictic breccia might be related to a rapid graben infill, with material supplied in part by exposed structural highs, mixed with reworked carbonate coming from the platform growing along the surrounding margin. In this context, the argillaceous sandstone above the breccia (facies L5) can be attributed to a later stage of the graben infill, probably in more distal conditions (Jiang et al., 2003b; Łabaj and Pratt, 2016). Therefore, such sequence of facies might represent a phase of intense continental erosion, alongside a steep topography related to extensional faulting, which triggered massive flows of sediments and their redeposition downslope. Here we revise the interpretation of Boggiani (1998), Fernandes and Boggiani (2021), who interpreted this deposit as associated to a regressive phase. Even though a relatively low sea level might have favored continental erosion, a steep topography and sufficient depth were necessary to accommodate such a thick sediment bed.

Carbonate deposition in the Laginha section begins with a sequence of facies L6 and L7, followed by L8 alternated with L9, L10, and L11. These facies can indicate a low energy environment, however, the presence of syn-sedimentary fractures and occasional brecciation suggests post depositional destabilization, possibly related to the still ongoing opening of the rift or to the gravitational slides onto a steep substrate (e.g., Sanders and Höfling, 2000; Basilone et al., 2016). The absence of fluidification and slumping structures makes more likely a gravitational than a seismic trigger (Audemard and Michetti, 2011) Consequently, the lenticular massive breccia devoid of basement clasts (facies L12), occurring between 5 and 10 m, can be related to a local sediment slide, with reworking of intraclasts, forming a small fan downdip (Ding et al., 2021). Besides, the calcimudstones with bird-eyes structures, occurring repeatedly above (facies L13), indicate shallow tidal or peritidal conditions, reached after the rapid filling of the graben in a still relatively low sea level phase (**Figures 6, 9**; Tucker and Wright, 1990; Burchette and Wright, 1992; Flügel, 2004; Ding et al., 2021).

The rhythmic marls and limestones (facies L14, L15) in the middle part of the Laginha section, show changes in the content of mud respect to skeletal grains (Oliveira, 2010; Fazio et al., 2019). The shifts between carbonate and siliciclastic deposition could have been driven by high frequency variation in relative sea level or climate in a mid-ramp environment (e.g., Schlager, 2005; Harper et al., 2015; Łabaj and Pratt, 2016). These alternating facies change gradually upward to marly intraclastic packstones (facies L16), representing a small shift back to inner ramp (Burchette and Wright, 1992).

The upper segment of the section consists of oolitic grainstones (facies L17), up until the contact with the mudstones of the Guaicurus Formation. The oolites are cemented by calcite and range in size from mid to coarse

TABLE 1 | Lithofacies and facies associations of the Corcal section.

Facies asociacion	Facies	Description	Process
Back-ramp to inner ramp carbonate platform	C1—Massive calcimudstone	Sets of decimeters thick wavy to tabular beds composed of massive dark gray carbonate mudstone. Local occurrence of bioclasts, intraclasts, interstitial concentration of clay and extraclasts (Qz, Op).	Settling of suspended micrite with episodic wave reworking and continental input.
	C2—Calcimudstone with desiccation features	Sets of centimetres to decimetres thick beds with wavy to tabular bedding, composed of massive, dark gray, carbonate mudstone with bird-eyes structures or chert filled cracks. Local occurrence of bioclasts, intraclasts and extraclasts (Qz, Ap, Bt, Op).	Settling of suspended micrite with episodic wave reworking, continental input, and emersion and desiccation.
	C3—Grainstone with elongated intraclasts	Grainstone in centimeters thick tabular beds composed of elongated micritic intraclasts and blocky calcite cement.	Micrite indurated and fragmented by desiccation and episodic wave reworking.
	C4—Marl	Centimeters to decimeters thick tabular beds with mixed siliciclastic and carbonate mud. From brown to light gray in color, massive to fissile.	Settling of suspended micrite and siliciclastic mud in shallow low-energy conditions.
Mid-ramp carbonate platform	C5—Packstone	Sets of centimeters to decimeters thick tabular to wavy beds of massive, dark gray packstone composed of intraclasts and bioclasts, mainly of <i>Cloudina</i> type organisms, in a micritic matrix. Local occurrence of sparse extraclasts, clay seams, nodules, and mild dolomitization.	Transport and reworking of sediments below the fair-weather wave base.
	C6—Grainstone	Sets of centimeters to decimeters thick tabular to wavy beds of massive dark gray grainstone composed of bioclasts, mainly of <i>Cloudina</i> type organisms, intraclasts, and oolites cemented by sparite.	Transport and reworking of sediments above the fair-weather wave base.
	C7—Intraclastic breccia	Centimeters thick tabular bed of recrystallized breccia composed of rounded, poorly sorted intraclasts in micritic matrix.	Highly reworked micritic or micritized grains redeposited below the fair-weather wave base.
Outer ramp carbonate platform	C8—Shale	Centimeters to metres thick tabular beds composed of massive to fissile siliciclastic mudstone, beige to gray, with calcite filled veins. Local occurrence of <i>C. wernerii</i> specimens and ichnofossils	Settling of suspended mud below the storm wave base.
Volcanic pulse	C9—Volcanic tuff	Centimeters thick tabular beds of whitish to yellowish claystone, very friable.	Volcanic ashes transported by winds and currents after the eruption and redeposited by settling or gravity flows.

sand, with a relatively thick carbonate coating, indicating a shallow, warm, high-energy environment (Sumner and Grotzinger, 1993). This facies can represent oolitic sand shoals in an inner ramp environment during a relatively high sea level phase, similar to the upper Corcal section (Figure 6; Tucker and Wright, 1990; Amorim et al., 2020; Ding et al., 2021).

Finally, the grayish mudstones of the Guaicurus Formation represent the facies L18. The fine grains size and the absence of carbonate constituents indicate very low energy condition and no carbonate input, similar to the facies C8 in the Corcal section. However, Fazio et al. (2019) noticed a different mineralogical composition and the absence of post burial deformation structures in the mudstone of the Guaicurus Formation, respect to the shales of the Corcal section. Besides, the yellowish beige siltstone with kaolinite and gypsum at the base of the Guaicurus Formation can indicate alteration by connate fluids or by post-depositional meteoric water interaction. All this evidence suggests a period of non-deposition prior to the onset of the Guaicurus Formation, during which the sediments of the Tamengo formation became altered (Fazio et al., 2019). This highlights the possibility of a hiatus occurring between the Tamengo and the Guaicurus formations.

5.2 Lateral and Temporal Variation in $\delta^{13}\text{C}$

The $\delta^{13}\text{C}$ values have no clear correlation with $\delta^{18}\text{O}$ in both studied sections, which indicates no significant alteration by early burial diagenesis even though some samples are recrystallized (Kaufman and Knoll, 1995; Derry, 2010). In addition, the isotopic values are not clustered according to the sedimentary facies. In the Corcal section there is little point-to-point variation and a clear increasing trend within the lower part, reaching values between 4‰ and 6‰ that occur steadily in the upper part. Overall, the $\delta^{13}\text{C}$ record of the Corcal section is consistent with that of Boggiani et al. (2010), Rivera (2019), and the values agree with those of upper Ediacaran sections worldwide, such as in Northwester Canada (Macdonald et al., 2013), South China (Jiang et al., 2007; Ding et al., 2020), Namibia (Halverson et al., 2005), and Oman (Cozzi et al., 2004). In general, the $\delta^{18}\text{O}$ values in the Corcal section are relatively heavier in the upper part of the section, as well as the $\delta^{13}\text{C}$. These general increasing trends are consistent with the interpretation of a relative rise in sea level from the lower to the upper section, suggested in Section 5.1.1, since a more active carbonate factory and a higher distance from the shore might increase the $\delta^{13}\text{C}$ and the $\delta^{18}\text{O}$ values (Immenhauser et al., 2003).

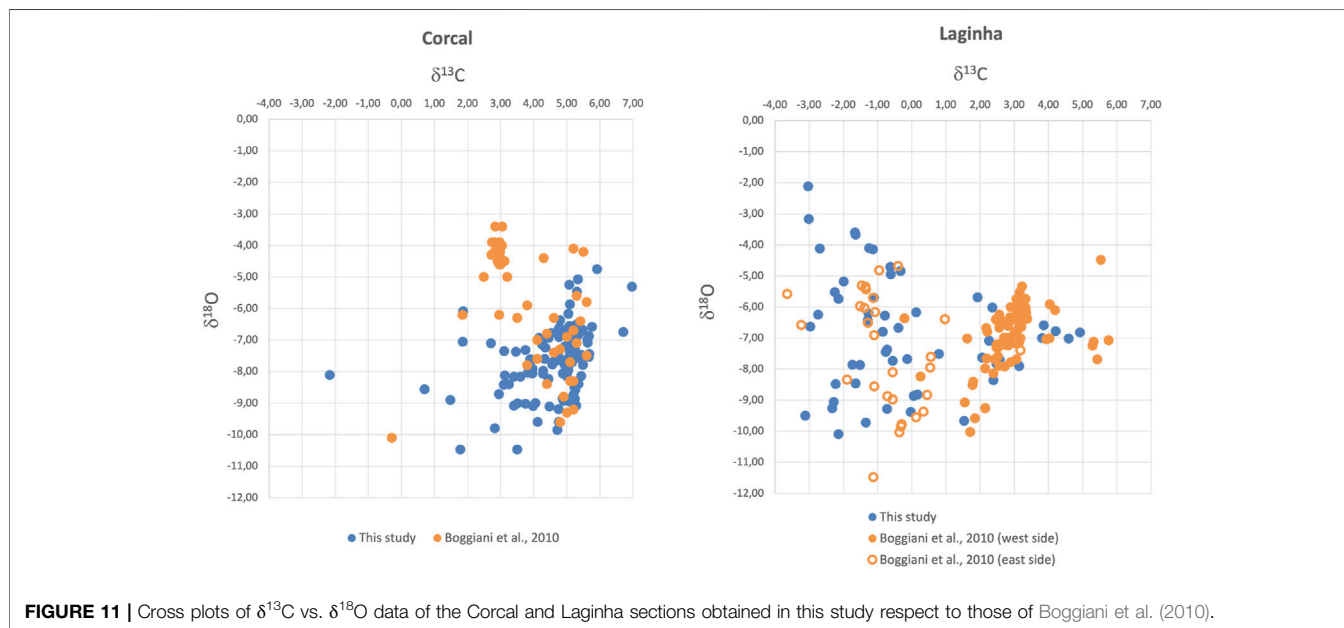
TABLE 2 | Lithofacies and facies associations of the Laginha section.

Facies association	Facies	Description	Process
Inner to mid-ramp carbonate platform	L1—Dolomitic grainstone	Meters thick tabular bed composed of massive light gray dolomitic grainstone.	Wave reworked sediment above the fair-weather wave base.
	L2—Sandstone with dolomitic matrix	Meters thick tabular bed composed of massive dark gray sandstone with dolomitic matrix. The grains are coarse sand sized, very well rounded, predominantly of quartz, with few lithoclasts.	Wave reworked sediment within the shoreface.
	L3—Peloidal packstone	~50 cm tabular bed composed of massive dark gray peloidal packstone with bird-eyes structures.	Low energy reworking in a shallow lagoon with episodic exposure.
Extensional tectonic and rapid accommodation space opening	L4—Polymictic breccia with basement clasts	Ten meters thick bed of massive polymictic breccia. The matrix is dark gray and dolomitic. Clasts range in size from sand to boulder, varying from rounded to very angular, and include limestones, dolostones, cherts, phosphorites, and granitoid rocks.	Rapid massive sediment flow onto a steep topography.
	L5—Argillaceous sandstone	Centimeters thick tabular bed composed of massive muddy sandstone, yellowish-brown when weathered, containing poorly sorted grains of quartz and lithoclast within an argillaceous matrix.	Massive siliciclastic sediment flow in deep and low energy conditions.
Inner ramp carbonate platform in a relatively steep and tectonically active setting	L6—Massive calcimudstone	Centimeters to decimeters thick tabular beds of massive gray carbonate mudstone, with sporadic extraclasts of quartz.	Settling of suspended micrite in shallow and restricted conditions with sporadic continental input.
	L7—Calcimudstone microbreccia	Centimeters thick beds of brecciated grey carbonate mudstone, with very angular clasts ranging in size from fine sand to gravel and cemented by syntaxial and eventually dog tooth calcite cement	Tectonic brecciation of micritic layers and subsequent early diagenetic cementation.
	L8—Dolomitic sparstone	Centimeters to decimetres thick tabular beds of massive to laminated, gray, crystalline dolostone, with extraclasts of quartz. Locally occurring fractures.	Sedimentation in shallow and restricted conditions with sporadic low energy currents reworking and continental input
	L9—Extraclastic wackestone	Centimeters to decimetres thick beds of light gray massive wackestone with poorly sorted quartz, mica, and phosphate grains, within a micritic matrix	Sedimentation in shallow and restricted conditions with continental input.
	L10—Intraclastic breccia	Centimeters thick weavy bed of massive breccia with poorly sorted and angular grains, with abundant extraclasts of quartz	Pulse of resedimented material with mixed (carbonate and siliciclastic) composition.
	L11—Laminated carbonate	Centimeters thick bed of gray fine crystalline, dolomitic to calcitic, carbonate laminae, alternated with poorly sorted siliciclastic laminae.	Settling of suspended micrite with pulses of siliciclastic material from the continent.
	L12—Polymictic intraclastic breccia	Meters thick lenticular bed of polymictic breccia with micritic, dark gray matrix. Clasts range in size from sand to pebble, vary in shape from rounded to angular, and include quartz, limestones, dolostones, siliciclastic mudstones, and phosphorites	Massive flow of reworked sediment from the shore, probably deposited as a local fan.
	L13—Calcimudstone with desiccation features	Centimeters to decimetres thick tabular beds composed of massive, gray, recrystallized carbonate mudstone with fenestral pores filled with spatic mosaic calcite, with local occurrence of micritization and silicified nodules.	Settling of micrite in very shallow conditions with episodes of emersion and desiccation.
Inner to mid-ramp carbonate platform	L14—Packstone	Decimeters thick bed of dark gray packstone with irregular intraclasts and <i>Cloudina</i> type bioclasts.	Transport and reworking of sediments below the fair-weather wave base.
	L15—Marl	Centimeters to decimetres thick beds with mixed siliciclastic and carbonate mud, occurring as thin layers within carbonate beds or as thick massive tabular beds.	Settling of suspended micrite and siliciclastic mud in shallow low-energy conditions.
	L16—Marly packstone	Decimeters thick bed of dark gray, massive marly intraclastic packstone, quite recrystallized,	

(Continued on following page)

TABLE 2 | (Continued) Lithofacies and facies associations of the Laginha section.

Facies associacion	Facies	Description	Process
	L17—Grainstone	with irregular intraclasts and possibly few <i>Cloudina</i> type bioclasts. Sets of decimeters thick beds of dark gray massive grainstone, mainly formed by oolites, and showing microstylolites.	Settling of suspended micrite with input of reworked carbonate grains from the surroundings. Transport and reworking of sediments above the fair-weather wave base.
Offshore siliciclastic setting	L18—Mudstone	Centimeters thick beds of laminated, beige mudstone.	Settling of siliciclastic mud in low energy conditions.

**FIGURE 11** | Cross plots of $\delta^{13}\text{C}$ vs. $\delta^{18}\text{O}$ data of the Corcal and Laginha sections obtained in this study respect to those of Boggiani et al. (2010).

On the other hand, the Laginha section displays $\delta^{13}\text{C}$ values more variable and generally 1‰–2‰ lower than those in the Corcal, especially in the lower and middle parts. However, there is no distinct relationship between $\delta^{13}\text{C}$ and sedimentary facies, lithology, or diagenetic features. Moreover, this variability can be observed laterally, as well as vertically. Boggiani et al. (2010) measured two profiles, one on the East and one on the West side of the Laginha quarry, which yielded significantly different values, despite representing the same stratigraphic interval (Figure 12). The profile of the Laginha section in this study corresponds to the West side of Boggiani et al. (2010), however, the data overlap with both profiles (Figure 11).

The different facies and $\delta^{13}\text{C}$ values of the Tamengo Formation in the two studied sections make also difficult to correlate them precisely. This becomes even more difficult as Ediacaran guide fossils, such as *C. lucianoii* and *C. wernerii*, were found only in the Corcal section, but lack in the Laginha (Adórno et al., 2017). This is due, in part, to the fact that the lower part of the Tamengo Fm. occurs only in the Laginha section, however, the upper part of this section should display $\delta^{13}\text{C}$ values that match those of the Corcal, which is not the case. The greater variability of $\delta^{13}\text{C}$ values in the Laginha section indicates a stronger influence by local environmental

or diagenetic factors in this section, respect to Corcal (Klein et al., 1999; Frank and Bernet, 2000; Spangenberg et al., 2014; Swart and Oehlert, 2018). Unraveling these factors is a complex work, which is beyond the goal of this study. However, it is important to stress that the $\delta^{13}\text{C}$ signal of the Laginha section is not representative of the general Ediacaran seawater and thus this section is not suitable for chemostratigraphic correlations. Previous studies chose the Laginha as reference section for correlation since it displays the entire Tamengo Formation, from the base to the top (Boggiani et al., 2010; Oliveira et al., 2019; Amorim et al., 2020). Our results show that the validity of these correlations must be re-assessed and that the Corcal section is a more suitable reference for stratigraphic correlation, despite not encompassing the entire unit.

The new $\delta^{13}\text{C}$ record of the Corcal section allows for enhancing the correlation of the Corumbá Group with the Arroyo del Soldado Group in Uruguay, which presumably deposited along the same continental margin (Gaucher et al., 2003). Considering the facies similarity, Gaucher et al. (2003) proposed that the Tamengo Formation could be correlated with the Polanco Formation of the Arroyo del Soldado Group. Adórno et al. (2019a) revised this correlation with a biostratigraphic

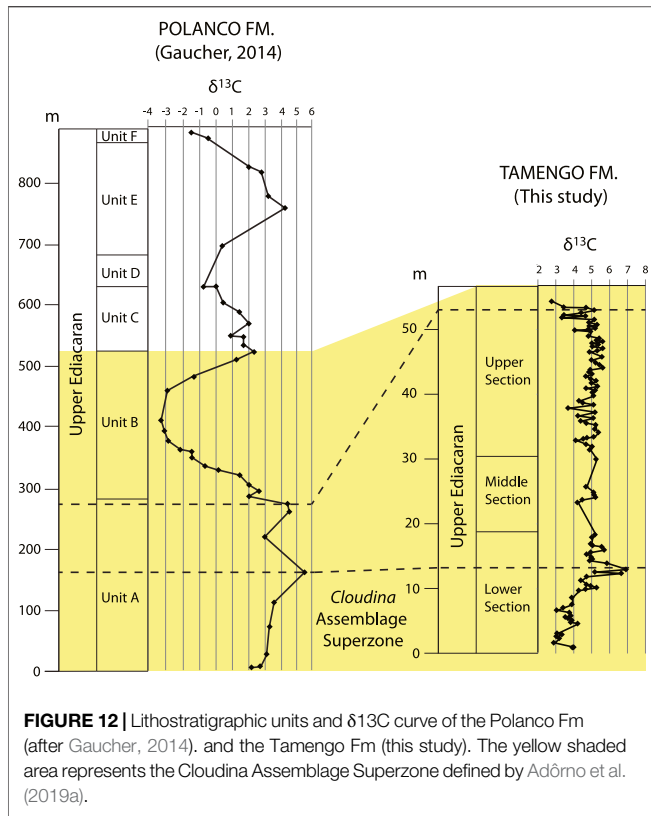


FIGURE 12 | Lithostratigraphic units and $\delta^{13}\text{C}$ curve of the Polanco Fm (after Gaucher, 2014), and the Tamengo Fm (this study). The yellow shaded area represents the Cloudina Assemblage Superzone defined by Adôrno et al. (2019a).

approach and showed that the Tamengo Formation is equivalent to the upper part of the Yermal Formation and the lower to middle part of the Polanco Formation. The $\delta^{13}\text{C}$ curve of the Polanco Formation shows three positive excursions, one in the lower and two in the upper part (Figure 12; Gaucher, 2014). By integrating the biostratigraphic data of Adôrno et al. (2019a) with the $\delta^{13}\text{C}$ data of Gaucher (2014) and of the Corcal section, the upper part of the Tamengo Formation turns

equivalent to the lower part of the Polanco Formation (Figure 12). According to this correlation, the upper Polanco, the Barriga Negra, and the Cerro Espulitas formations of the Arroyo del Soldado Group should be equivalent to the uppermost part of the Tamengo Formation and to the lower part of the Guaicurus Formation, suggesting that the uppermost part of the Ediacaran is very condensed in the Corumbá Group. However, it is also possible that an unconformity occurs between the Tamengo and the Guaicurus formations (Adôrno et al., 2019a; Fazio et al., 2019).

5.3 Tamengo Formation Depositional Model

Previous studies proposed that the Tamengo Formation deposited as a ramp carbonate platform onto a passive margin (Boggiani et al., 2010; Oliveira et al., 2019; Amorim et al., 2020). According to this model the Laginha section represents the shallower part of the carbonate platform, whereas the Corcal section the mid- and outer parts. The clastic lithofacies and the cross and hummocky stratification indicate an environment controlled mainly by waves and storms (Dott and Bourgeois, 1982; Seguret et al., 2001; Dumas and Arnott, 2006; Amorim et al., 2020). However, here we identified desiccation features in the lower part of the Corcal section, indicating that the environment reached also back- to inner ramp conditions (Tucker and Wright, 1990; Burchette and Wright, 1992; Tucker and Dias-Brito, 2017). Consequently, the carbonate ramp of the Tamengo Formation shifted from a back-ramp to an outer ramp setting, represented by the C2 and C8 facies, respectively (Table 1). This implies an environment more dynamic than previously thought, strongly controlled by sea level fluctuations, as well as by waves and storms.

This has also important implications for constraining the dwelling conditions of the Ediacaran organisms *C. luciano* and *C. werner*, of which fossils have been recovered in the Corcal and in the correlative Sobramil section (Adôrno et al., 2017; Walde et al., 2015; Oliveira et al., 2019; Amorim et al.,

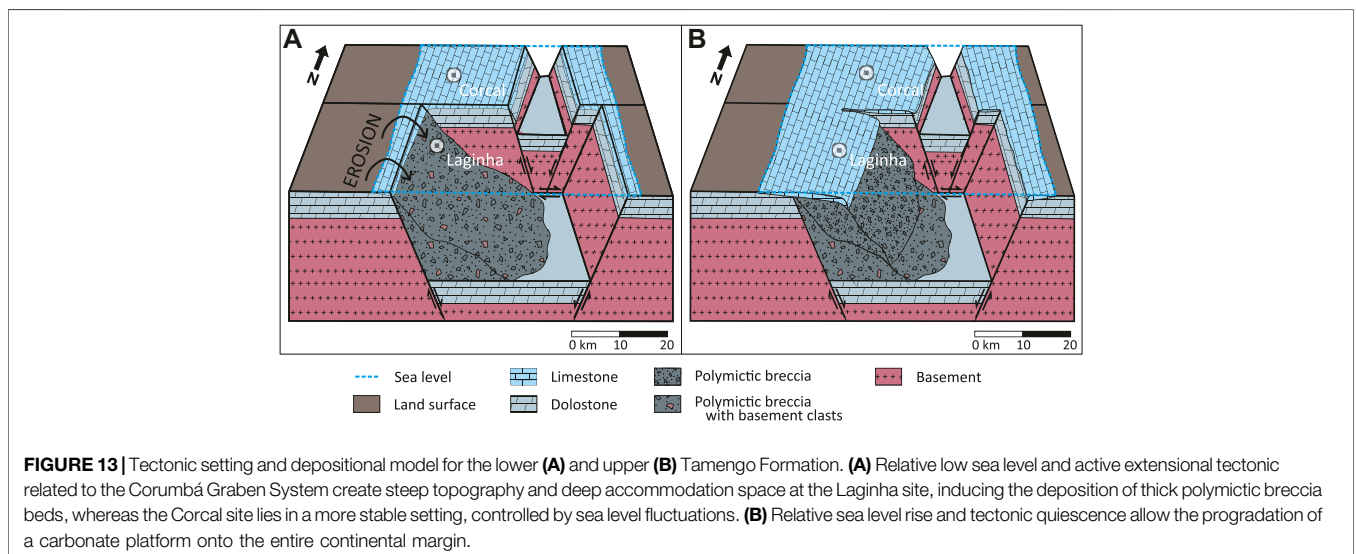


FIGURE 13 | Tectonic setting and depositional model for the lower (A) and upper (B) Tamengo Formation. (A) Relative low sea level and active extensional tectonic related to the Corumbá Graben System create steep topography and deep accommodation space at the Laginha site, inducing the deposition of thick polymictic breccia beds, whereas the Corcal site lies in a more stable setting, controlled by sea level fluctuations. (B) Relative sea level rise and tectonic quiescence allow the progradation of a carbonate platform onto the entire continental margin.

2020). The occurrence of these fossils is strongly facies dependent, as *Cloudina* type fragments have been observed in the packstone and grainstone facies, whereas *C. weneri* occurs only in the shales. This indicates shifting ecological conditions in response to sea level variations, with *C. weneri* proliferating in a deeper environment, with lower energy and a softer and finer substrate, during transgressive phases. On the other hand, *C. luciano* became dominant in shallower and higher energy conditions, therefore with more light and nutrients availability, during high stands (Sanders and Pons, 1999; Walde et al., 2015; Oliveira et al., 2019; Amorim et al., 2020; Li et al., 2021).

The “classical” facies of the Tamengo Formation are those observed in the Corcal section, which occur also in other outcrops of the region along the Paraguay river, such as in the sections of Porto Sobramil (also known as Claudio or Saladeiro), Cacimba, Porto Figueiras, Goldfish, Ladario-Corumbá escarpment, and Horii mine (Boggiani et al., 2010; Walde et al., 2015; Adórno et al., 2019b; Oliveira et al., 2019; Rivera, 2019; Amorim et al., 2020). Alongside the same lithofacies, these sections display also consistent and rather homogenous $\delta^{13}\text{C}$ values (Boggiani et al., 2010; Rivera, 2019; Caetano Filho, 2020; and this work). These facies are different from those observed in the Laginha section, and therefore the Laginha was considered from a more proximal setting than the Corcal and other sections along the Paraguay river (Boggiani et al., 2010; Oliveira et al., 2019; Amorim et al., 2020). However, previous studies focus only on the upper part of the Tamengo Formation and do not consider the thick breccia layers in the Laginha section. In fact, as discussed in the facies interpretation, these breccias, are meters to tens of meters thick, homogeneous, and polymictic, indicating a deposition by mass sediment flows. Therefore, it was necessary a steep topography for triggering the flow and sufficient space to accommodate tens of meters of sediment at once. These conditions contrast with a shallow inner carbonate ramp. Besides, the more variable facies sequence of the Laginha section indicates a more dynamic environment, influenced by other factors alongside waves and sea level variations.

A steep topography and a rapidly opening accommodation space can be found in setting dominated by extensional tectonic (e.g., Sanders and Höfling, 2000; Eyles and Januszczak, 2007). In this context can occur also basement uplift, which provides coarse, angular, and fresh clasts such as those occurring in the lower part of the Laginha section. Warren et al. (2019) propose a model for the basin evolution of the Itapucumi Group, in Paraguay, which outcrops about 250 km to the South of Corumbá and is correlative to the Corumbá Group. According to this model, at the time of deposition of the Tamengo Fm (ca 555 to 542 Ma) the basin was in a thermal subsidence regime, during a post-rift stage, but still influenced by extensional tectonic. Therefore, the carbonate platform of the Tamengo Formation formed onto an irregular margin, with a complex topography, controlled by extensional faults (i.e., Figure 13A, Sanders and Höfling, 2000; Ding et al., 2021). In this context, the Corcal section corresponds to a more stable portion of the ramp, not significantly influenced by the tectonic. On the other hand, the Laginha section sat close to or into the margin of a graben,

with a steep topography, and next to a horst that provided the terrigenous supply. Therefore, the Corcal section was not necessarily further from the shore than the Laginha, but just laid onto a flatter and smoother topography (Figure 13A). The upper part of the Tamengo Formation consists of mid-ramp carbonate facies in both studied sections. Consequently, according to this interpretation, it can represent a period of tectonic quiescence, during which the relative sea level rose. This could have favored the progradation of the carbonate platform, which leveled the topography (e.g., Figure 13B, Tucker and Wright, 1990; Sanders and Pons, 1999; Schlager, 2005; Łabaj and Pratt, 2016).

This interpretation can explain the more variable facies and stable isotopes records of the Laginha section. A steep and tectonically active setting can be more susceptible to changes in input of continental material, local currents, and even burial fluids, which might have contributed to the dolomitization of the lower part of the section (Caetano Filho, 2020). It can also explain the absence of *C. weneri* remains in the Laginha section, as a steep topography and the input of coarse material might have precluded the installation of quite conditions and fine substrate necessary for these organisms. Therefore, the Laginha section represents an exceptional setting for the Tamengo Formation, strongly influenced by local factors both in the lithological and in the stable isotopes' records.

5.4 Implications for Ediacaran Paleoenvironments

The Tamengo Formation contains allochemical and bioclastic constituents typical of Ediacaran carbonate ramps (e.g., Sumner and Grotzinger, 1993; Narbonne et al., 1994; Walter et al., 1995; Grotzinger and James, 2000; Gaucher et al., 2003; Jiang et al., 2003b; Lindsay et al., 2005; Jiang et al., 2011; Xiao et al., 2016; Vaziri and Laflamme, 2018; Warren et al., 2019; Álvaro et al., 2020). On the other hand, the detail facies analysis presented here allows for unraveling more specific characteristics of its depositional environment.

Differently from some of the most renowned coeval carbonate successions, such as the Nama Group in Namibia, the Little Dal Group in northwestern Canada, the Buah Formation in Oman, and even the closest Bambuí Group in Brazil, the Tamengo Formation consists of totally clastic lithofacies, with no biogenic buildups (Batten et al., 2004; Cozzi et al., 2004; Grotzinger et al., 2005; Alvarenga et al., 2014; Uhlein et al., 2019). Microbial laminations have been observed only sporadically as reworked intraclasts in the breccia facies. *Cloudina* type skeletal fragments are frequent, but no specimens have been found in place. However, the abundance of micritic matrix and intraclasts indicates the presence of a developed biogenic carbonate factory. Moreover, recent evidence of microalgae, preserved in shale facies, indicate a diversified biotic assemblage (Diniz et al., 2021). Amorim et al. (2020) explain this apparent paradox suggesting that frequent storms and currents might have prevented the formation of extensive biogenic carbonate buildups, or that the shallower part, in which the carbonate producers dwelled, was not preserved. We agree that the high energy might have contributed, but consider unlikely the non-preservation of carbonate reefs and buildups, as they generally

have the higher potential of preservation (e.g., Tucker and Wright, 1990; Schlager, 2005).

The Tamengo Formation yields lithofacies like those of the Doushantuo and Dengying formations, which form an extensive, well preserved, and well-studied Ediacaran carbonate platforms system onto the Yangtze block, in South China. There, the sediments of the carbonate ramp are preserved with lateral continuity, from the inner shelf to the basin (Jiang et al., 2011; Ding et al., 2019; Ding et al., 2021). This indicates that Ediacaran carbonate platforms were heterogeneous and the presence of subtidal stromatolites, thrombolites, or even metazoan reefs is not necessarily a prerogative. Even though the availability of the outcrops in the Corumbá region is not as high as that in South China, we can infer that the Tamengo Formation was a “Doushantuo- Dengying type” carbonate platform, characterized by a productive carbonate factory, but with environmental conditions that did not allow the deposition of significant buildups with a biogenic framework. This could be due to particularly high energy, but also to temperature, salinity, or nutrients conditions (Tucker and Wright, 1990; Schlager, 2005). In the case of the Tamengo Formation, the presence of extraclasts in several layers suggest the possibility of runoff that episodically decreased the salinity and increased the trophic level of the environment. Besides, especially in the Laginha section, a steep topography might have limited the space with favorable ecological conditions for growing biogenic reefs. It is interesting to note that also the upper Ediacaran Dengying Fm. formed in a setting controlled by extensional tectonic (Ding et al., 2021).

6 CONCLUSION

In this work we present new evidence from two representative sections of the Tamengo Formation. This unit consists of carbonate and subordinate siliciclastic lithofacies, deposited onto a continental platform during the Ediacaran. The two studied sections display different lithofacies and carbonate carbon isotope values, despite belonging to the same lithostratigraphic unit. The previously proposed depositional model attributed this difference to the distance from the shoreline, considering the Laginha section more proximal than the Corcal. Here, we propose that the Laginha site was not necessarily more proximal, but characterized by a steeper topography, which provided the accommodation for the thick breccia bed in the lower part of the section. Such context could have been due to active normal faults at the time of the deposition, indicating that the platform laid on a tectonically active margin. If this were true, then the Laginha section could provide indirect evidence that the Corumbá Graben System was still active at the time of the Tamengo Formation.

We show that the Laginha section is more heterogeneous and discontinuous than the Corcal section, despite displaying both the base and the top of the Tamengo Formation. The $\delta^{13}\text{C}$ record is also more dispersed, suggesting a major influence by local and post depositional factors. On the other hand, the Corcal section yields a more continuous $\delta^{13}\text{C}$ record, with typical Ediacaran values, as well as Ediacaran guide fossils, which allow for a more accurate stratigraphic calibration. Therefore, despite not

encompassing the entire unit, the Corcal section is a more suitable reference for stratigraphic correlations.

By comparing the Tamengo Formation with other Ediacaran carbonate platforms, we observe the absence of biogenic carbonate buildups, which, instead, are common in other coeval units. The facies of the Tamengo Formation are like those of the Doushantuo and Dengying formations, in South China, suggesting that the Ediacaran carbonate platforms could have been more heterogeneous than previously thought. These differences might have been due to different ecological conditions, such as energy, temperature, salinity, or nutrients.

Our results advance in the characterization of the Ediacaran in South America, which is still at a lower level compared to other regions, and highlight the Tamengo Formation as a possible reference unit. Moreover, we show the importance of detailed petrographic and geochemical characterization, alongside facies analyses, to unravel the still enigmatic Ediacaran carbonate paleoenvironments and their significance at regional to global scale.

DATA AVAILABILITY STATEMENT

The original contributions presented in the study are included in the article/**Supplementary Material**, further inquiries can be directed to the corresponding author.

AUTHOR CONTRIBUTIONS

MR—Fieldwork, data collection and interpretation, drawing of the figures and writing of the manuscript. MG—Master supervisor of MR fieldwork, data interpretation, drawing of the figures and writing of the manuscript. DW—Fieldwork and access to the studied sites, data interpretation, review of the manuscript for the regional and stratigraphic context. DC—Access to the thin sections of the Ediacariano project and to the optical microscope laboratory, review of the paleontological and stratigraphic aspects of the manuscript. GF—Fieldwork, review of the diagenetic aspects of the manuscript. LV—Part of the stable isotopes measurements, review of the geochemical aspects of the manuscript. MD—Fieldwork, samples organization, review of the paleontological and stratigraphic aspects of the manuscript. RS—Chief of the stable isotope geochemistry laboratory, assistance with the stable isotopes measurements and data interpretation, review of the geochemical aspects of the manuscript. RA—Fieldwork, assistance with the fossils' data, review of the paleontological and stratigraphic aspects of the manuscript. LG—Bachelor student supervised by MG review of the stratigraphic correlation of the Tamengo Formation with the Arroyo del Soldado Group.

FUNDING

Main funding came from the Research Foundation of the Federal District (FAPDF)—process no. 0193.001609/2017, and the FUNDECT/CNPq/DCR—process no. 59/300.349/2016. This study was financed in part by the Coordenação de

Aperfeiçoamento de Pessoal de Nível Superior—Brasil (CAPES)—Finance Code 001. Part of the studied samples were obtained from the project “Arcabouço cronobioestratigráfico do Ediacariano do Brasil através do desenvolvimento metodológico em paleontologia – EDIACARIANO”, funded by ANP & PETROBRAS, N. PETROBRAS/FUB-IG-2012/5005.

ACKNOWLEDGMENTS

The authors thank André Pullen of the Stable Isotopes Laboratory of the University of Brasilia for the technical support with stable isotope analysis; the administration and personnel of the Corcal and Votorantin that allowed the access to the Corcal and Laginha

quarries, respectively; Bernie D. Erdtmann for the helpful discussions and assistance during fieldwork; Aguinaldo Silva of the Federal University of Mato Grosso do Sul and CEPAN for the logistical support in Corumbá. We are also thankful to the associate editor MC and to four reviewers, who contributed with insightful and constructive comments.

SUPPLEMENTARY MATERIAL

The Supplementary Material for this article can be found online at: <https://www.frontiersin.org/articles/10.3389/feart.2022.749066/full#supplementary-material>

REFERENCES

- Adórno, R. R., do Carmo, D. A., Germs, G., Walde, D. H. G., Denezine, M., Boggiani, P. C., et al. (2017). *Cloudina Lucianoi* (Beurlen & Sommer, 1957), Tamengo Formation, Ediacaran, Brazil: Taxonomy, Analysis of Stratigraphic Distribution and Biostratigraphy. *Precambrian Res.* 301, 19–35. doi:10.1016/j.precamres.2017.08.023
- Adórno, R. R. (2019). Taxonomy, Paleocology and Chronobiostratigraphy across the Ediacaran-Cambrian Boundary: Tamengo and Guaicurus Formations. Doctoral thesis. Brasilia: University of Brasilia, 130.
- Adórno, R. R., Walde, D. H. G., Do Carmo, D. A., Denezine, M., Cortijo, I., Sanchez, E. A. M., et al. (2019a). Análisis Paleontológicos a Través Límite Ediacárico-Cámbrico, Grupo Alto Corumbá, Brasil. *Estud. Geol.* 75 (2), 094. doi:10.3989/egol.43586.549
- Adórno, R. R., Walde, D. H. G., Erdtmann, B. D., Denezine, M., Cortijo, I., Do Carmo, D. A., et al. (2019b). First Occurrence of *Cloudina* Carinata Cortijo et al., 2010 in South America, Tamengo Formation, Corumbá Group, Upper Ediacaran of Midwestern. *Estud. Geol.* 75 (2), 095. doi:10.3989/egol.43587.550
- Almeida, F. F. M. (1965). Geologia da Serra da Bodoquena (Mato Grosso), Brasil. *Bol. Geol. Mineral. DNP* 219, 1–96.
- Almeida, F. F. M. (1964). Geologia Do Sudoeste Mato-Grossense. *Bol. Div. Geol. Mineral. DNP* 116, 1–18.
- Almeida, F. F. M. (1984). “Provincia Tocantins, Setor Sudoeste,” in *O Pré-Cambriano Do Brasil*. Editors F.F.M. de Almeida and Y. Hasui (São Paulo: Edgard Blücher), 265–281.
- Alvarenga, C. J., Boggiani, P. C., Babinski, M., Dardenne, M. A., Figueiredo, M. F., Dantas, E. L., et al. (2011). *Glacially Influenced Sedimentation of the Puga Formation, Cuiabá Group and Jacadigo Group, and Associated Carbonates of the Araras and Corumbá Groups, Paraguay Belt, Brazil*. London, Memoirs: Geological Society 36 (1), 487–497. doi:10.1144/M36.45
- Alvarenga, C. J. S., Santos, R. V., Vieira, L. C., Lima, B. A. F., and Mancini, L. H. (2014). Meso-Neoproterozoic Isotope Stratigraphy on Carbonates Platforms in the Brasilia Belt of Brazil. *Precambrian Res.* 251, 164–180. doi:10.1016/j.precamres.2014.06.011
- Álvaro, J. J., Cortijo, I., Jensen, S., Mus, M. M., and Palacios, T. (2020). *Cloudina*-Microbial Reef Resilience to Substrate Instability in a Cadomian Retro-Arc Basin of the Iberian Peninsula. *Precambrian Res.* 336, 105479. doi:10.1016/j.precamres.2019.105479
- Amorim, K. B., Afonso, J. W. L., Leme, J. d. M., Diniz, C. Q. C., Rivera, L. C. M., Gómez-Gutiérrez, J. C., et al. (2020). Sedimentary Facies, Fossil Distribution and Depositional Setting of the Late Ediacaran Tamengo Formation (Brazil). *Sedimentology* 67 (7), 3422–3450. doi:10.1111/sed.12749
- Audemard, F. A. M., and Michetti, A. M. (2011). Geological Criteria for Evaluating Seismicity Revisited: Forty Years of Paleoseismic Investigations and the Natural Record of Past Earthquakes. *Geol. Soc. Am. Special Pap.* 479, 1–21. doi:10.1130/2011.2479(00)
- Babinski, M., Boggiani, P. C., Fanning, M., Simon, C. M., and Sial, A. N. (2008). “U–Pb Shrimp Geochronology and Isotope Chemostratigraphy (C, O, Sr) of the Tamengo Formation, Southern Paraguay Belt,” in 6th South American Symposium on Isotope Geology San Carlos de Bariloche, San Carlos de Bariloche, 2008 160.
- Babinski, M., Boggiani, P. C., Trindade, R. I. F., and Fanning, C. M. (2013). Detrital Zircon Ages and Geochronological Constraints on the Neoproterozoic Puga Diamictites and Associated BIFs in the Southern Paraguay Belt, Brazil. *Gondwana Res.* 23, 988–997. doi:10.1016/j.gr.2012.06.011
- Basilone, L., Sulli, A., and Gasparo Morticelli, M. (2016). The Relationships Between Soft-Sediment Deformation Structures and Syndimentary Extensional Tectonics in Upper Triassic Deep-Water Carbonate Succession (Southern Tethyan Rifted Continental Margin - Central Sicily). *Sediment. Geol.* 344, 310–322. doi:10.1016/j.sedgeo.2016.01.010
- Batten, K. L., Narbonne, G. M., and James, N. P. (2004). Paleoenvironments and Growth of Early Neoproterozoic Calcimicrobial Reefs: Platformal Little Dal Group, Northwestern Canada. *Precambrian Res.* 133 (3-4), 249–269. doi:10.1016/j.precamres.2004.05.003
- Becker-Kerber, B., Pacheco, M. L. A. F., Rudnitzki, I. D., Galante, D., Rodrigues, F., and Leme, J. d. M. (2017). Ecological Interactions in *Cloudina* from the Ediacaran of Brazil: Implications for the Rise of Animal Biomineralization. *Sci. Rep.* 7, 5482. doi:10.1038/s41598-017-05753-8
- Beurlen, K., and Sommer, F. W. (1957). Observações estratigráficas e paleontológicas sobre o calcário de Corumbá. *Bol. Geol. Mineral.-DNP* 168, 1–35.
- Boggiani, P. C., and Alvarenga, C. J. S. (2004). “Faixa Paraguai,” in *Geologia do Continente Sul-Americano: Evolução da Obra de Fernando Flávio Marques de Almeida*. Editors V. Mantesso-Neto, A. Bartorelli, C.D.R. Carneiro, and B.B.B. Neves (São Paulo: Beca Produções Culturais Ltda), 113–120.
- Boggiani, P. C. (1998). Análise Estratigráfica da Bacia Corumbá (Neoproterozoico) – Mato Grosso do Sul. Ph.D. Thesis. Brasil: Universidade de São Paulo, 1–181.
- Boggiani, P. C., Fairchild, T. R., and Coimbra, A. M. (1993). O Grupo Corumbá (Neoproterozoico-Cambriano) Na Região Central Da Serra Da Bodoquena (Faixa Paraguai), Mato Grosso Do Sul. *Rbg* 23, 301–305. doi:10.25249/0375-7536.1993233301305
- Boggiani, P. C., Gaucher, C., Sial, A. N., Babinski, M., Simon, C. M., Riccomini, C., et al. (2010). Chemostratigraphy of the Tamengo Formation (Corumbá Group, Brazil): A Contribution to the Calibration of the Ediacaran Carbon-Isotope Curve. *Precambrian Res.* 182, 382–401. doi:10.1016/j.precamres.2010.06.003
- Bristow, T. F., and Kennedy, M. J. (2008). Carbon Isotope Excursions and the Oxidant Budget of the Ediacaran Atmosphere and Ocean. *Geol.* 36 (11), 863–866. doi:10.1130/g24968a.1
- Burchette, T. P., and Wright, V. P. (1992). Carbonate Ramp Depositional Systems. *Sediment. Geol.* 79, 3–57. doi:10.1016/0037-0738(92)90003-a
- Caetano Filho, S. (2020). Carbon and Sulfur Biogeochemical Cycles in the Brazilian Ediacaran Record. Doctoral dissertation. São Paulo: Universidade de São Paulo, 629.
- Campanha, G. A. d. C., Boggiani, P. C., Sallun Filho, W., Sá, F. R. d., Zuquim, M. d. P. S., and Piacentini, T. (2011). A faixa de dobramento Paraguai na Serra da Bodoquena e depressão Do Rio Miranda, Mato Grosso Do Sul. *Geol. USP. Sér. Cient.* 11, 79–96. doi:10.5327/z1519-874x2011000300005

- Canfield, D. E., Poulton, S. W., and Narbonne, G. M. (2007). Late-Neoproterozoic Deep-Ocean Oxygenation and the Rise of Animal Life. *Science* 315 (5808), 92–95. doi:10.1126/science.1135013
- Chen, Z.-Q., Tu, C., Pei, Y., Ogg, J., Fang, Y., Wu, S., et al. (2019). Biosedimentological Features of Major Microbe-Metazoan Transitions (MMTs) from Precambrian to Cenozoic. *Earth-Science Rev.* 189, 21–50. doi:10.1016/j.earscirev.2019.01.015
- Cozzi, A., Grotzinger, J. P., and Allen, P. A. (2004). Evolution of a Terminal Neoproterozoic Carbonate Ramp System (Buah Formation, Sultanate of Oman): Effects of Basement Paleotopography. *Geol. Soc. Am. Bull.* 116 (11–12), 1367–1384. doi:10.1130/b25387.1
- Crockford, P. W., Cowie, B. R., Johnston, D. T., Hoffman, P. F., Sugiyama, I., Pellerin, A., et al. (2016). Triple Oxygen and Multiple Sulfur Isotope Constraints on the Evolution of the Post-Marinoan Sulfur Cycle. *Earth Planet. Sci. Lett.* 435, 74–83. doi:10.1016/j.epsl.2015.12.017
- Cui, H., Kaufman, A. J., Peng, Y., Liu, X.-M., Plummer, R. E., and Lee, E. I. (2018). The Neoproterozoic Hüttenberg $\delta^{13}\text{C}$ Anomaly: Genesis and Global Implications. *Precambrian Res.* 313, 242–262. doi:10.1016/j.precamres.2018.05.024
- Cui, H., Kitajima, K., Orland, I. J., Xiao, S., Baele, J.-M., Kaufman, A. J., et al. (2021). Deposition or Diagenesis? Probing the Ediacaran Shuram Excursion in South China by SIMS. *Glob. Planet. Change* 206, 103591. doi:10.1016/j.gloplacha.2021.103591
- D’el-Rey Silva, L. J. H., Walde, D. H.-G., and Saldanha, D. O. (2016). The Neoproterozoic-Cambrian Paraguay Belt, Central Brazil: Part I - New Structural Data and a New Approach on the Regional Implications. *Tectonophysics* 676, 20–41. doi:10.1016/j.tecto.2016.03.019
- De Alvarenga, C. J. S., Boggiani, P. C., Babinski, M., Dardenne, M. A., Figueiredo, M., Santos, R. V., et al. (2009). “Chapter 2 the Amazonian Palaeocontinent,” in *Neoproterozoic-Cambrian Tectonics, Global Changes and Evolution: A Focus on Southwestern Gondwana*. Editors C. Gaucher, A.N. Sial, H. Frimmel, and G.P. Halverson (Amsterdam: Elsevier), 15–28. doi:10.1016/s0166-2635(09)01602-8
- de Alvarenga, C. J. S., and Trompette, R. (1992). Glacially Influenced Sedimentation in the Later Proterozoic of the Paraguay Belt (Mato Grosso, Brazil). *Palaeogeogr. Palaeoclimatol. Palaeoecol.* 92, 85–105. doi:10.1016/0031-0182(92)90136-s
- Delgado, F. (1977). Primary Textures in Dolostones and Recrystallized Limestones: a Technique for Their Microscopy Study. *J. Sediment. Petrology* 47, 1339–1341.
- Delpomdor, F., Eyles, N., Tack, L., and Pr at, A. (2016). Pre- and Post-Marinoan Carbonate Facies of the Democratic Republic of the Congo: Glacially- or Tectonically-Influenced Deep-Water Sediments? *Palaeogeogr. Palaeoclimatol. Palaeoecol.* 457, 144–157. doi:10.1016/j.palaeo.2016.06.014
- Derry, L. A. (2010). A Burial Diagenesis Origin for the Ediacaran Shuram-Wonoka Carbon Isotope Anomaly. *Earth Planet. Sci. Lett.* 294, 152–162. doi:10.1016/j.epsl.2010.03.022
- Ding, Y., Chen, D., Zhou, X., Guo, C., Huang, T., and Zhang, G. (2019). Tectono-Depositional Pattern and Evolution of the Middle Yangtze Platform (South China) During the Late Ediacaran. *Precambrian Res.* 333, 105426. doi:10.1016/j.precamres.2019.105426
- Ding, Y., Chen, D., Zhou, X., Huang, T., Guo, C., and Yeasmin, R. (2020). Paired $\delta^{13}\text{C}_{\text{carb}}$ - $\delta^{13}\text{C}_{\text{org}}$ Evolution of the Dengying Formation from Northeastern Guizhou and Implications for Stratigraphic Correlation and the Late Ediacaran Carbon Cycle. *J. Earth Sci.* 31 (2), 342–353. doi:10.1007/s12583-018-0886-1
- Ding, Y., Li, Z., Liu, S., Song, J., Zhou, X., Sun, W., et al. (2021). Sequence Stratigraphy and Tectono-Depositional Evolution of a Late Ediacaran Epeiric Platform in the Upper Yangtze Area, South China. *Precambrian Res.* 354, 106077. doi:10.1016/j.precamres.2020.106077
- Diniz, C., Leme, J., and Boggiani, P. C. (2021). New Species of Macroalgae from Tamengo Formation, Ediacaran, Brazil. *Front. Earth Sci.* 9, 884. doi:10.3389/feart.2021.748876
- Dott, R. H., Jr, and Bourgeois, J. (1982). Hummocky Stratification: Significance of its Variable Bedding Sequences. *Geol. Soc. Am. Bull.* 93 (8), 663–680. doi:10.1130/0016-7606(1982)93<663:hssoiv>2.0.co;2
- Dumas, S., and Arnott, R. W. C. (2006). Origin of Hummocky and Swaley Cross-Stratification- the Controlling Influence of Unidirectional Current Strength and Aggradation Rate. *Geol.* 34 (12), 1073–1076. doi:10.1130/g22930a.1
- Elie, M., Nogueira, A. C. R., N ed elec, A., Trindade, R. I. F., and Kenig, F. (2007). A Red Algal Bloom in the Aftermath of the Marinoan Snowball Earth. *Terra nova.* 19 (5), 303–308. doi:10.1111/j.1365-3121.2007.00754.x
- Eyles, N., and Januszczak, N. (2007). Syntectonic Subaqueous Mass Flows of the Neoproterozoic Otavi Group, Namibia: Where Is the Evidence of Global Glaciation? *Basin Res.* 19 (2), 179–198. doi:10.1111/j.1365-2117.2007.00319.x
- Fairchild, T. R. (1978). “Evid ncias paleontol gicas de uma poss vel idade Ediacariana ou Cambriana Inferior, para a parte leste Do Grupo Corumb  (Mato Grosso Do Sul),” in *30o Congresso Brasileiro de Geologia, Recife, 1978, 181. Resumo das Comunica es.*
- Fazio, G., Guimar es, E. M., Walde, D. W. G., Do Carmo, D. A., Adorno, R. R., Vieira, L. C., et al. (2019). Mineralogical and Chemical Composition of Ediacaran-Cambrian Pelitic Rocks of the Tamengo and Guaicurus Formations, (Corumb  Group - MS, Brazil): Stratigraphic Positioning and Paleoenvironmental Interpretations. *J. S. Am. Earth Sci.* 90, 487–503. doi:10.1016/j.jsames.2018.11.025
- Fernandes, H. A., and Boggiani, P. C. (2021). “Brecha polim tica basal da Forma o Tamengo (Grupo Corumb ): Sedimentologia, proveni ncia e correla o com outras unidades ediacaranas,” in *Anais 50 CBG-Congresso Brasileiro de Geologia, 2020, June 28–30, 2021, 1.*
- Fike, D. A., Grotzinger, J. P., Pratt, L. M., and Summons, R. E. (2006). Oxidation of the Ediacaran Ocean. *Nature* 444, 744–747. doi:10.1038/nature05345
- Fl gel, E. (2004). *Microfacies of Carbonate Rocks: Analysis, Interpretation and Application*. Germany: Springer-Verlag Berlin Heidelberg, 976.
- Fontanela, G. T. (2012). Dolomitiza o e Fosfog nese na Forma o Bocaina, Grupo Corumb  (Ediacarano). Disserta o (Mestrado). S o Paulo: Instituto de Geoci ncias, Universidade de S o Paulo, 148.
- Frank, T. D., and Bernet, K. (2000). Isotopic Signature of Burial Diagenesis and Primary Lithological Contrasts in Periplatform Carbonates (Miocene, Great Bahama Bank). *Sedimentology* 47 (6), 1119–1134. doi:10.1046/j.1365-3091.2000.00344.x
- Frimmel, H. E. (2010). On the Reliability of Stable Carbon Isotopes for Neoproterozoic Chemostratigraphic Correlation. *Precambrian Res.* 182 (4), 239–253. doi:10.1016/j.precamres.2010.01.003
- Gan, T., Luo, T., Pang, K., Zhou, C., Zhou, G., Wan, B., et al. (2021). Cryptic Terrestrial Fungus-Like Fossils of the Early Ediacaran Period. *Nat. Commun.* 12 (1), 1–12. doi:10.1038/s41467-021-20975-1
- Gaucher, C., Boggiani, P. C., Sprechmann, P., Sial, A. N., and Fairchild, T. R. (2003). Integrated correlation of the Vendian to Cambrian Arroyo del Soldado and Corumb  Groups (Uruguay and Brazil): Palaeogeographic, Palaeoclimatic and Palaeobiologic Implications. *Precambrian Res.* 120, 241–278. doi:10.1016/s0301-9268(02)00140-7
- Gaucher, C. (2014). Grupo Arroyo del Soldado. *Geol. del Urug.* 1 (16), 313–339.
- Gernon, T. M., Hincks, T. K., Tyrrell, T., Rohling, E. J., and Palmer, M. R. (2016). Snowball Earth Ocean Chemistry Driven by Extensive Ridge Volcanism During Rodinia Breakup. *Nat. Geosci.* 9, 242–248. doi:10.1038/ngeo2632
- Gorjan, P., Veevers, J. J., and Walter, M. R. (2000). Neoproterozoic Sulfur-Isotope Variation in Australia and Global Implications. *Precambrian Res.* 100 (1-3), 151–179. doi:10.1016/s0301-9268(99)00073-x
- Grant, V. J. (1990). Maternal Personality and Sex of Infant. *Am. J. Sci.* 63, 261–266. doi:10.1111/j.2044-8341.1990.tb01618.x
- Grotzinger, J., Adams, E. W., and Schr der, S. (2005). Microbial-Metazoan Reefs of the Terminal Proterozoic Nama Group (C. 550–543 Ma), Namibia. *Geol. Mag.* 142 (5), 499–517. doi:10.1017/s0016756805000907
- Grotzinger, J. P., Fike, D. A., and Fischer, W. W. (2011). Enigmatic Origin of the Largest-Known Carbon Isotope Excursion in Earth’s History. *Nat. Geosci.* 4, 285–292. doi:10.1038/ngeo1138
- Grotzinger, J. P., and James, N. P. (2000). “Precambrian Carbonates: Evolution of Understanding,” in *Carbonate Sedimentation and Diagenesis in the Evolving Precambrian World* (Tulsa, OK: SEPM Special Publication), 67. doi:10.2110/pec.00.67.0003
- Grotzinger, J. P., and Knoll, A. H. (1995). Anomalous Carbonate Precipitates: Is the Precambrian the Key to the Permian? *Palaios* 10, 578–596. doi:10.2307/3515096
- Hahn, G., Hahn, R., Leonardos, O. H., Pflug, H. D., and Walde, D. H. G. (1982). Korperlich Erhaltene Scyphozoen-Reste aus dem Jungprakambrium Brasiliens. *Geol. Palaeontol.* 16, 1–18.
- Halverson, G. P., Hoffman, P. F., Schrag, D. P., Maloof, A. C., and Rice, A. H. N. (2005). Toward a Neoproterozoic Composite Carbon-Isotope Record. *Geol. Soc. Am. Bull.* 117, 1181–1207. doi:10.1130/b25630.1
- Halverson, G. P., and Hurtgen, M. T. (2007). Ediacaran Growth of the Marine Sulfate Reservoir. *Earth Planet. Sci. Lett.* 263 (1-2), 32–44. doi:10.1016/j.epsl.2007.08.022

- Halverson, G. P., Wade, B. P., Hurtgen, M. T., and Barovich, K. M. (2010). Neoproterozoic Chemostratigraphy. *Precambrian Res.* 182, 337–350. doi:10.1016/j.precamres.2010.04.007
- Harper, B. B., Puga-Bernabéu, Á., Drozler, A. W., Webster, J. M., Gischler, E., Tiwari, M., et al. (2015). Mixed Carbonate-Siliciclastic Sedimentation Along the Great Barrier Reef Upper Slope: A Challenge to the Reciprocal Sedimentation Model. *J. Sediment. Res.* 85 (9), 1019–1036. doi:10.2110/jsr.2015.58.1
- Hidalgo, R. L. L. (2002). Análise micropaleontológica das formações Tamengo e Guaicurus, Grupo Corumbá (MS), e Formação Araras (MT), transição do Neoproterozóico-Fanerozóico. Dissertação (Mestrado). São Paulo: Instituto de Geociências, Universidade de São Paulo.
- Hoffman, P. F., Kaufman, A. J., Halverson, G. P., and Schrag, D. P. (1998). A Neoproterozoic Snowball Earth. *Science* 281, 1342–1346. doi:10.1126/science.281.5381.1342
- Hohl, S. V., Becker, H., Herzlieb, S., and Guo, Q. (2015). Multiproxy Constraints on Alteration and Primary Compositions of Ediacaran Deep-Water Carbonate Rocks, Yangtze Platform, South China. *Geochimica Cosmochimica Acta* 163, 262–278. doi:10.1016/j.gca.2015.04.037
- Hu, Y., Cai, C., Liu, D., Pederson, C. L., Jiang, L., Shen, A., et al. (2020). Formation, Diagenesis and Palaeoenvironmental Significance of Upper Ediacaran Fibrous Dolomite Cements. *Sedimentology* 67 (2), 1161–1187. doi:10.1111/sed.12683
- Hurtgen, M. T., Arthur, M. A., and Halverson, G. P. (2005). Neoproterozoic Sulfur Isotopes, the Evolution of Microbial Sulfur Species, and the Burial Efficiency of Sulfide as Sedimentary Pyrite. *Geol.* 33 (1), 41–44. doi:10.1130/g20923.1
- Husson, J. M., Linzmeier, B. J., Kitajima, K., Ishida, A., Maloof, A. C., Schoene, B., et al. (2020). Large Isotopic Variability at the Micron-Scale in ‘Shuram’ Excursion Carbonates from South Australia. *Earth Planet. Sci. Lett.* 538, 116211. doi:10.1016/j.epsl.2020.116211
- Immenhauser, A., Della Porta, G., Kenter, J. A. M., and Bahamonde, J. R. (2003). An Alternative Model for Positive Shifts in Shallow-Marine Carbonate $\delta^{13}\text{C}$ and $\delta^{18}\text{O}$. *Sedimentology* 50 (5), 953–959. doi:10.1046/j.1365-3091.2003.00590.x
- Jiang, G., Christie-Blick, N., Kaufman, A. J., Banerjee, D. M., and Rai, V. (2003b). Carbonate Platform Growth and Cyclicity at a Terminal Proterozoic Passive Margin, Infra Krol Formation and Krol Group, Lesser Himalaya, India. *Sedimentology* 50 (5), 921–952. doi:10.1046/j.1365-3091.2003.00589.x
- Jiang, G., Kaufman, A. J., Christie-Blick, N., Zhang, S., and Wu, H. (2007). Carbon Isotope Variability Across the Ediacaran Yangtze Platform in South China: Implications for a Large Surface-To-Deep Ocean $\delta^{13}\text{C}$ Gradient. *Earth Planet. Sci. Lett.* 261 (1–2), 303–320. doi:10.1016/j.epsl.2007.07.009
- Jiang, G., Kennedy, M. J., and Christie-Blick, N. (2003a). Stable Isotopic Evidence for Methane Seeps in Neoproterozoic Postglacial Cap Carbonates. *Nature* 426 (6968), 822–826. doi:10.1038/nature02201
- Jiang, G., Shi, X., Zhang, S., Wang, Y., and Xiao, S. (2011). Stratigraphy and Paleogeography of the Ediacaran Doushantuo Formation (Ca. 635–551Ma) in South China. *Gondwana Res.* 19 (4), 831–849. doi:10.1016/j.gr.2011.01.006
- Johnston, D. T., Macdonald, F. A., Gill, B. C., Hoffman, P. F., and Schrag, D. P. (2012). Uncovering the Neoproterozoic Carbon Cycle. *Nature* 483 (7389), 320–323. doi:10.1038/nature10854
- Jones, J. P. (1985). The Southern Border of the Guaporé Shield in Western Brazil and Bolivia: An Interpretation of its Geologic Evolution. *Precambrian Res.* 28, 111–135. doi:10.1016/0301-9268(85)90076-2
- Kaufman, A. J. (2018). “The Ediacaran-Cambrian Transition: A Resource-Based Hypothesis for the Rise and Fall of the Ediacara Biota,” in *Chemostratigraphy Across Major Chronological Boundaries*. Editors A. N. Sial, C. Gaucher, M. Ramkumar, and V. Pinto Ferreira. First Edition, 115–142. *Geophysical Monograph* 240 (Washington, DC: John Wiley & Sons, Inc.). doi:10.1002/9781119382508.ch7
- Kaufman, A., and Knoll, A. (1995). Neoproterozoic Variations in the C-Isotopic Composition of Seawater: Stratigraphic and Biogeochemical Implications. *Precambrian Res.* 73, 27–49. doi:10.1016/0301-9268(94)00070-8
- Kennedy, M., Mrofka, D., and Von Der Borch, C. (2008). Snowball Earth Termination by Destabilization of Equatorial Permafrost Methane Clathrate. *Nature* 453 (7195), 642–645. doi:10.1038/nature06961
- Kerber, B. B., Rosa, A. L. Z. d., Gabas, S. G., Leme, J. d. M., and Pacheco, M. L. A. F. (2013). O registro fossilífero de metazoários ediacaranos na América Do Sul e suas implicações nos estudos sobre origem e complexificação da vida animal. *Geol. Usp. Sér. Cient.* 13 (3), 51–64. doi:10.5327/z1519-874x201300030006
- Klein, J. S., Mozley, P., Campbell, A. R., and Cole, R. (1999). Spatial Distribution of Carbon and Oxygen Isotopes in Laterally Extensive Carbonate-Cemented Layers; Implications for Mode of Growth and Subsurface Identification. *J. Sediment. Res.* 69 (1), 184–201. doi:10.2110/jsr.69.184
- Knoll, A. H., and Carroll, S. B. (1999). Early Animal Evolution: Emerging Views from Comparative Biology and Geology. *Science* 284, 2129–2137. doi:10.1126/science.284.5423.2129
- Laakso, T. A., Sperling, E. A., Johnston, D. T., and Knoll, A. H. (2020). Ediacaran Reorganization of the Marine Phosphorus Cycle. *Proc. Natl. Acad. Sci. U.S.A.* 117 (22), 11961–11967. doi:10.1073/pnas.1916738117
- Łabaj, M. A., and Pratt, B. R. (2016). Depositional Dynamics in a Mixed Carbonate-Siliciclastic System: Middle-Upper Cambrian Abrigo Formation, Southeastern Arizona, U.S.A. *J. Sediment. Res.* 86 (1), 11–37. doi:10.2110/jsr.2015.96
- Laschet, C. (1984). On the Origin of Cherts. *Facies* 10, 257–289. doi:10.1007/bf02536693
- Le Heron, D. P., and Craig, J. (2012). Neoproterozoic Deglacial Sediments and Their Hydrocarbon Source Rock Potential. *Geol. Soc. Lond. Spec. Publ.* 368 (1), 381–393. doi:10.1144/sp368.16
- Lenton, T. M., Boyle, R. A., Poulton, S. W., Shields-Zhou, G. A., and Butterfield, N. J. (2014). Co-Evolution of Eukaryotes and Ocean Oxygenation in the Neoproterozoic Era. *Nat. Geosci.* 7 (4), 257–265. doi:10.1038/ngeo2108
- Li, H., Li, F., Li, X., Zeng, K., Gong, Q., Yi, C., et al. (2021). Development and Collapse of the Early Cambrian Shallow-Water Carbonate Factories in the Hannan-Micangshan Area, South China. *Palaeogeogr. Palaeoclimatol. Palaeoecol.* 583, 110665. doi:10.1016/j.palaeo.2021.110665
- Li, Z.-X., Evans, D. A. D., and Halverson, G. P. (2013). Neoproterozoic Glaciations in a Revised Global Palaeogeography from the Breakup of Rodinia to the Assembly of Gondwanaland. *Sediment. Geol.* 294, 219–232. doi:10.1016/j.sedgeo.2013.05.016
- Lindsay, J. F., Kruse, P. D., Green, O. R., Hawkins, E., Brasier, M. D., Cartlidge, J., et al. (2005). The Neoproterozoic–Cambrian Record in Australia: A Stable Isotope Study. *Precambrian Res.* 143 (1–4), 113–133. doi:10.1016/j.precamres.2005.10.002
- Lloyd, S. J., Marenco, P. J., Hagadorn, J. W., Lyons, T. W., Kaufman, A. J., Sour-Tovar, F., et al. (2012). Sustained Low Marine Sulfate Concentrations from the Neoproterozoic to the Cambrian: Insights from Carbonates of Northwestern Mexico and Eastern California. *Earth Planet. Sci. Lett.* 339–340, 79–94. doi:10.1016/j.epsl.2012.05.032
- Macdonald, F. A., Strauss, J. V., Sperling, E. A., Halverson, G. P., Narbonne, G. M., Johnston, D. T., et al. (2013). The Stratigraphic Relationship Between the Shuram Carbon Isotope Excursion, the Oxygenation of Neoproterozoic Oceans, and the First Appearance of the Ediacara Biota and Bilaterian Trace Fossils in Northwestern Canada. *Chem. Geol.* 362, 250–272. doi:10.1016/j.chemgeo.2013.05.032
- Meira, F. V. E. (2011). Caracterização tafonômica e estratigráfica de *Cloudina lucianoi* (Beurlen e Sommer, 1957) Zaine e Fairchild, 1985, no Grupo Corumbá, Ediacarano do Brasil. Dissertação (Mestrado). São Paulo: Instituto de Geociências, Universidade de São Paulo.
- Narbonne, G. M., Kaufman, A. J., and Knoll, A. H. (1994). Integrated Chemostratigraphy and Biostratigraphy of the Windermere Supergroup, Northwestern Canada: Implications for Neoproterozoic Correlations and the Early Evolution of Animals. *Geol. Soc. Am. Bull.* 106 (10), 1281–1292. doi:10.1130/0016-7606(1994)106<1281:icabot>2.3.co;2
- Narbonne, G. M., Xiao, S., Shields, G. A., and Gehling, J. G. (2012). The Ediacaran Period. *Geol. Time Scale* 1, 413–435. doi:10.1016/b978-0-444-59425-9.00018-4
- Nichols, G. (2009). *Sedimentology and Stratigraphy*. Oxford: John Wiley & Sons.
- Och, L. M., and Shields-Zhou, G. A. (2012). The Neoproterozoic Oxygenation Event: Environmental Perturbations and Biogeochemical Cycling. *Earth-Science Rev.* 110, 26–57. doi:10.1016/j.earscirev.2011.09.004
- Oliveira, R. S. (2010). Depósitos de rampa carbonática Ediacarana do Grupo Corumbá, região de Corumbá, Mato Grosso do Sul. Dissertação (Mestrado). Belém: Instituto de Geociências, Universidade Federal do Pará.
- Oliveira, R. S. d., Nogueira, A. C. R., Romero, G. R., Truckenbrodt, W., and da Silva Bandeira, J. C. (2019). Ediacaran Ramp Depositional Model of the Tamengo Formation, Brazil. *J. S. Am. Earth Sci.* 96, 102348. doi:10.1016/j.jsames.2019.102348

- Parry, L. A., Boggiani, P. C., Condon, D. J., Garwood, R. J., Leme, J. d. M., McLroy, D., et al. (2017). Ichnological Evidence for Meiofaunal Bilaterians from the Terminal Ediacaran and Earliest Cambrian of Brazil. *Nat. Ecol. Evol.* 1, 1455–1464. doi:10.1038/s41559-017-0301-9
- Penny, A. M., Wood, R., Curtis, A., Bowyer, F., Tostevin, R., and Hoffman, K.-H. (2014). Ediacaran Metazoan Reefs from the Nama Group, Namibia. *Science* 344, 1504–1506. doi:10.1126/science.1253393
- Piacentini, T., Vasconcelos, P. M., and Farley, K. A. (2013). $^{40}\text{Ar}/^{39}\text{Ar}$ Constraints on the Age and Thermal History of the Urucum Neoproterozoic Banded Iron-Formation, Brazil. *Precambrian Res.* 228, 48–62. doi:10.1016/j.precamres.2013.01.002
- Ramos, M. E. A. F., Giorgioni, M., do Carmo, D. A., Walde, D. H. G., Guimarães, E. M., Fazio, G., et al. (2019). Chemostratigraphic and Facies Characterization of Ediacaran Platform Carbonates (Tamengo Formation, Corumbá Group): Preliminary Results. *Estudios Geológicos* 75 (2), e111. doi:10.3989/egcol.43589.566
- Riding, R., and Virgone, A. (2020). Hybrid Carbonates: *In Situ* Abiotic, Microbial and Skeletal Co-Precipitates. *Earth-Science Rev.* 208, 103300. doi:10.1016/j.earscirev.2020.103300
- Ries, J. B., Fike, D. A., Pratt, L. M., Lyons, T. W., and Grotzinger, J. P. (2009). Superheavy Pyrite ($\delta^{34}\text{S}_{\text{pyr}} > \delta^{34}\text{S}_{\text{SCAS}}$) in the Terminal Proterozoic Nama Group, Southern Namibia: A Consequence of Low Seawater Sulfate at the Dawn of Animal Life. *Geology* 37 (8), 743–746. doi:10.1130/g25775a.1
- Rivera, L. C. M. (2019). C and O Isotopes of the Middle and Upper Tamengo Formation (Corumbá Group-Upper Ediacaran): Effects of the Sedimentary Facies and Diagenesis. Master dissertation. Universidade de São Paulo, 824.
- Sanders, D., and Höfling, R. (2000). Carbonate Deposition in Mixed Siliciclastic-Carbonate Environments on Top of an Orogenic Wedge (Late Cretaceous, Northern Calcareous Alps, Austria). *Sediment. Geol.* 137 (3–4), 127–146. doi:10.1016/s0037-0738(00)00084-1
- Sanders, D., and Pons, J. M. (1999). Rudist Formations in Mixed Siliciclastic-Carbonate Depositional Environments, Upper Cretaceous, Austria: Stratigraphy, Sedimentology, and Models of Development. *Palaeogeogr. Palaeoclimatol. Palaeoecol.* 148 (4), 249–284. doi:10.1016/s0031-0182(98)00186-2
- Schlager, W. (2005). *Carbonate Sedimentology and Sequence Stratigraphy* (No. 8). Tulsa, OK: SEPM Society for Sedimentary Geology.
- Seguret, M., Moussine-Pouchkine, A., Gabaglia, G. R., and Bouchette, F. (2001). Storm Deposits and Storm-Generated Coarse Carbonate Breccias on a Pelagic Outer Shelf (South-East Basin, France). *Sedimentology* 48 (2), 231–254. doi:10.1046/j.1365-3091.2001.00358.x
- Shields, G. A., Mills, B. J. W., Zhu, M., Raub, T. D., Daines, S. J., and Lenton, T. M. (2019). Unique Neoproterozoic Carbon Isotope Excursions Sustained by Coupled Evaporite Dissolution and Pyrite Burial. *Nat. Geosci.* 12 (10), 823–827. doi:10.1038/s41561-019-0434-3
- Sial, A. N., Gaucher, C., Misi, A., Boggiani, P. C., Alvarenga, C. J. S. d., Ferreira, V. P., et al. (2016). Correlations of Some Neoproterozoic Carbonate-Dominated Successions in South America Based on High-Resolution Chemostratigraphy. *Braz. J. Geol.* 46 (3), 439–488. doi:10.1590/2317-4889201620160079
- Spangenberg, J. E., Bagnoud-Velásquez, M., Boggiani, P. C., and Gaucher, C. (2014). Redox Variations and Bioproductivity in the Ediacaran: Evidence from Inorganic and Organic Geochemistry of the Corumbá Group, Brazil. *Gondwana Res.* 26, 1186–1207. doi:10.1016/j.gr.2013.08.014
- Sumner, D. Y., and Grotzinger, J. P. (1993). Numerical Modeling of Ooid Size and the Problem of Neoproterozoic Giant Ooids. *J. Sediment. Pet.* 63 (5), 974–982. doi:10.1306/d4267c5d-2b26-11d7-8648000102c1865d
- Swart, P. K., and Oehlert, A. M. (2018). Revised Interpretations of Stable C and O Patterns in Carbonate Rocks Resulting from Meteoric Diagenesis. *Sediment. Geol.* 364, 14–23. doi:10.1016/j.sedgeo.2017.12.005
- Thallner, D., Biggin, A. J., and Halls, H. C. (2021). An Extended Period of Extremely Weak Geomagnetic Field Suggested by Palaeointensities from the Ediacaran Grenville Dykes (SE Canada). *Earth Planet. Sci. Lett.* 568, 117025. doi:10.1016/j.epsl.2021.117025
- Tobias, T. C. (2014). Micropaleontologia da Formação Tamengo, Eco Parque Cacimba da Saúde, Ediacarano, Grupo Corumbá, Estado de Mato Grosso do Sul. Dissertação (Mestrado). Brasília: Instituto de Geociências, Universidade de Brasília, 88.
- Tostevin, R., He, T., Turchyn, A. V., Wood, R. A., Penny, A. M., Bowyer, F., et al. (2017). Constraints on the Late Ediacaran Sulfur Cycle from Carbonate Associated Sulfate. *Precambrian Res.* 290, 113–125. doi:10.1016/j.precamres.2017.01.004
- Trompette, R., de Alvarenga, C. J. S., and Walde, D. (1998). Geological Evolution of the Neoproterozoic Corumbágraben System (Brazil). Depositional Context of the Stratified Fe and Mn Ores of the Jacadigo Group. *J. S. Am. Earth Sci.* 11, 587–597. doi:10.1016/s0895-9811(98)00036-4
- Tucker, M. E., and Dias-Brito, D. (2017). *Petrologia Sedimentar Carbonática: Iniciação Com Base No Registro Geológico Do Brasil*, 3. Rio Claro, Obra: UNESP-IGCE-Unispetro, 208.
- Tucker, M. E., and Wright, V. P. (1990). *Carbonate Sedimentology*. Oxford: Blackwell Science.
- Uhlein, G. J., Uhlein, A., Pereira, E., Caxito, F. A., Okubo, J., Warren, L. V., et al. (2019). Ediacaran Paleoenvironmental Changes Recorded in the Mixed Carbonate-Siliciclastic Bambuí Basin, Brazil. *Palaeogeogr. Palaeoclimatol. Palaeoecol.* 517, 39–51. doi:10.1016/j.palaeo.2018.12.022
- Vaziri, S. H., and Laflamme, M. (2018). Lithostratigraphy and Sedimentary Environment of the Precambrian Kushk Series of Central Iran. *Can. J. Earth Sci.* 55 (11), 1284–1296. doi:10.1139/cjes-2017-0234
- Walde, D. H.-G., Weber, B., Erdtmann, B. D., and Steiner, M. (2019). Taphonomy of Corumbella Werneri from the Ediacaran of Brazil: Sinotubulid Tube or Conulariid Test? *Alcheringa Australas. J. Palaeontol.* 43, 335–350. doi:10.1080/03115518.2019.1615551
- Walde, D. H. G. (1988). *Das Proterozoische Paraguay-Araguaia Orogen in West-Brasilien, Ausgehend von Untersuchungen im Raum Corumbá*. *Habil. Schrift.* Freiburg: Albert-Ludwigs-Universität, 122.
- Walde, D. H. G., Do Carmo, D. A., Guimarães, E. M., Vieira, L. C., Erdtmann, B.-D., Sanchez, E. A. M., et al. (2015). New Aspects of Neoproterozoic-Cambrian Transition in the Corumbá Region (State of Mato Grosso Do Sul, Brazil). *Ann. Paléontologie* 101, 213–224. doi:10.1016/j.annpal.2015.07.002
- Walde, D. H. G., Leonardos, O. H., Hahn, G., Hahn, R., and Pflug, H. (1982). The First Precambrian Megafossil from South America, *Corumbella Werneri*. *An. Acad. Bras. Ciências* 54, 461.
- Walker, R. G. (1984). “Shelf and Shallow Marine Sands,” in *Facies Models*. Editor R.G. Walker (Canada: Geological Association of Canada), 141–170.
- Walter, M. R., Veevers, J. J., Calver, C. R., and Grey, K. (1995). Neoproterozoic Stratigraphy of the Centralian Superbasin, Australia. *Precambrian Res.* 73 (1–4), 173–195. doi:10.1016/0301-9268(94)00077-5
- Wang, J., La Croix, A. D., Wang, H., Guo, F., and Ren, B. (2019). Linkage Between Calcirudite Lithofacies and Storm-Generated Depositional Processes in the Upper Cambrian Series, Shandong Province, Eastern China. *Sediment. Geol.* 391, 105518. doi:10.1016/j.sedgeo.2019.105518
- Warren, L. V., Freitas, B. T., Riccomini, C., Boggiani, P. C., Quaglio, F., Simões, M. G., et al. (2019). Sedimentary Evolution and Tectonic Setting of the Itapucumi Group, Ediacaran, Northern Paraguay: From Rodinia Break-Up to West Gondwana Amalgamation. *Precambrian Res.* 322, 99–121. doi:10.1016/j.precamres.2018.12.022
- Wei, G.-Y., Hood, A. v. S., Chen, X., Li, D., Wei, W., Wen, B., et al. (2019). Ca and Sr Isotope Constraints on the Formation of the Marinoan Cap Dolostones. *Earth Planet. Sci. Lett.* 511, 202–212. doi:10.1016/j.epsl.2019.01.024
- Wentworth, C. K. (1922). A Scale of Grade and Class Terms for Clastic Sediments. *J. Geol.* 30 (5), 377–392. doi:10.1086/622910
- Wright, V. P. (1992). A Revised Classification of Limestones. *Sediment. Geol.* 76, 177–185. doi:10.1016/0037-0738(92)90082-3
- Xiao, S., Cui, H., Kang, J., McFadden, K. A., Kaufman, A. J., Kitajima, K., et al. (2020). Using SIMS to Decode Noisy Stratigraphic $\delta^{13}\text{C}$ Variations in Ediacaran Carbonates. *Precambrian Res.* 343, 105686. doi:10.1016/j.precamres.2020.105686
- Xiao, S., Narbonne, G. M., Zhou, C., Laflamme, G., Grahndankin, M. D. V., Grahndankin, D. V., Moczydłowska-Vidal, M., et al. (2016). Towards an Ediacaran Time Scale: Problems, Protocols, and Prospects. *Episodes* 39 (4), 540–555. doi:10.18814/epiugs/2016/v39i4/103886
- Yu, W., Algeo, T. J., Zhou, Q., Du, Y., and Wang, P. (2020). Cryogenian Cap Carbonate Models: A Review and Critical Assessment. *Palaeogeogr. Palaeoclimatol. Palaeoecol.* 552, 109727. doi:10.1016/j.palaeo.2020.109727

- Zaine, M. F. (1991). Análise dos fósseis de parte da Faixa Paraguai (MS, MT) e seu contexto temporal e paleoambiental. Ph.D. Thesis. Brazil: University of São Paulo, 218.
- Zaine, M. F., and Fairchild, T. R. (1985). Comparison of *Aulophycus Lucianoi* Beurlen & Sommer from Ladário (MS) and the Genus *Cloudina* Germs, Ediacaran of Namibia. *An. Acad. Bras. Ciências* 57, 1.
- Zhang, F., Xiao, S., Kendall, B., Romaniello, S. J., Cui, H., Meyer, M., et al. (2018). Extensive Marine Anoxia During the Terminal Ediacaran Period. *Sci. Adv.* 4 (6), eaan8983. doi:10.1126/sciadv.aan8983

Conflict of Interest: The authors declare that the research was conducted in the absence of any commercial or financial relationships that could be construed as a potential conflict of interest.

Publisher's Note: All claims expressed in this article are solely those of the authors and do not necessarily represent those of their affiliated organizations, or those of the publisher, the editors and the reviewers. Any product that may be evaluated in this article, or claim that may be made by its manufacturer, is not guaranteed or endorsed by the publisher.

Copyright © 2022 Ramos, Giorgioni, Walde, do Carmo, Fazio, Vieira, Denezine, V. Santos, R. Adorno and Lage Guida. This is an open-access article distributed under the terms of the Creative Commons Attribution License (CC BY). The use, distribution or reproduction in other forums is permitted, provided the original author(s) and the copyright owner(s) are credited and that the original publication in this journal is cited, in accordance with accepted academic practice. No use, distribution or reproduction is permitted which does not comply with these terms.